

Sulfoglycodendrimer Therapeutics for HIV-1 and SARS-CoV-2

Lauren Wells, Cory Vierra, Janee' Hardman, Yanxiao Han, Dustin Dimas, Lucia N. Gwarada-Phillips, Rachel Blackeye, Daryl K. Eggers, Celia C. LaBranche, Petr Král,* and Katherine D. McReynolds*

Hexavalent sulfoglycodendrimers (SGDs) are synthesized as mimics of host cell heparan sulfate proteoglycans (HSPGs) to inhibit the early stages in viral binding/entry of HIV-1 and SARS-CoV-2. Using an HIV neutralization assay, the most promising of the seven candidates are found to have sub-micromolar anti-HIV activities. Molecular dynamics simulations are separately implemented to investigate how/where the SGDs interacted with both pathogens. The simulations revealed that the SGDs: 1) develop multivalent binding with polybasic regions within and outside of the V3 loop on glycoprotein 120 (gp120) for HIV-1, and consecutively bind with multiple gp120 subunits, and 2) interact with basic amino acids in both the angiotensin-converting enzyme 2 (ACE2) and HSPG binding regions of the Receptor Binding Domain (RBD) from SARS-CoV-2. These results illustrate the considerable potential of SGDs as inhibitors in viral binding/entry of both HIV-1 and SARS-CoV-2 pathogens, leading the way for further development of this class of molecules as broad-spectrum antiviral agents.

been lost due to the rapid emergence of pathogens in major modern pandemics, such as the 1918 “Spanish” Flu (H1N1 influenza virus, 40 million deaths), Acquired Immunodeficiency Syndrome (AIDS) caused by the Human Immunodeficiency Virus (HIV), and now, COVID-19 (coronavirus disease-2019) caused by the coronavirus, SARS-CoV-2 (severe acute respiratory syndrome coronavirus 2). Currently, there are approximately 38 million people living with HIV/AIDS, 1.7 million new infections in 2019, and 32.7 million lives lost since the first reported case in 1981.^[1] For the rapidly emerging pandemic involving the coronavirus, SARS-CoV-2, over 100 million cases of COVID-19 have occurred, with over two million deaths reported since December of 2019.^[2]

In addition to the pursuit of effective vaccines against such pathogens as

1. Introduction

Pathogens capable of causing pandemics have been present throughout recorded human history. Millions of lives have

HIV-1 and SARS-CoV-2, it is important to have effective broad-spectrum antiviral drugs capable of minimizing transmission to those uninfected and easing/shortening disease symptoms. For influenza, oseltamivir and zanamivir, better known as Tamiflu and Relenza, can be prescribed when someone is in the early symptomatic stage of infection as a means to diminish symptoms, shorten the duration, and minimize the risk of death. This is particularly useful when one considers that the flu vaccine is only 40–60% effective and that only 45% of adults were vaccinated in the 2018–19 flu season.^[3] For HIV-1, pre-exposure prophylaxis (PrEP) has been developed for high-risk populations, as a way to minimize the sexual transmission of the virus, and consists of a single pill daily of Truvada, containing a combination of the drugs emtricitabine and tenofovir. However, this preventative method has not been widely adopted, and there have also been several reports of breakthrough infections.^[4] For SARS-CoV-2, there are two vaccines by Pfizer and Moderna that recently gained emergency use approval from the FDA. However, beyond the vaccines, there are currently only two drugs approved for critical COVID-19 cases, the antiviral drug, remdesivir, and the corticosteroid, dexamethasone. We still have a long way to go to get the COVID-19 pandemic under control. Herd immunity will take time to develop, and even with widespread vaccination people will still get infected with COVID-19, as even the current vaccines are not 100% effective. Presently, there are still rising levels of infections, hospitalizations, and death among

L. Wells, C. Vierra, J. Hardman, D. Dimas, L. N. Gwarada-Phillips, R. Blackeye, Prof. K. D. McReynolds
Department of Chemistry
California State University
Sacramento, 6000 J Street, Sacramento, CA 95819–6057, USA
E-mail: kdmcr@csus.edu

Dr. Y. Han, Prof. P. Král
Department of Chemistry
University of Illinois
Chicago 845 W. Taylor St., Chicago, IL 60607, USA
E-mail: pkral@uic.edu

Prof. P. Král
Departments of Physics, Pharmaceutical Sciences, and Chemical Engineering
University of Illinois
Chicago 845 W. Taylor St., Chicago, IL 60607, USA

Prof. D. K. Eggers
Department of Chemistry
San José State University
One Washington Square, San José, CA 95192, USA

Prof. C. C. LaBranche
Department of Surgery
Duke University
Durham, NC 27710, USA

DOI: 10.1002/adtp.202000210

patients. Clearly, we need to further explore the antiviral drug landscape in the hopes of finding reliable ways to reduce the infection rates of HIV-1 and SARS-CoV-2, such that the pandemics can be controlled.

The early stages of viral binding and entry for both HIV-1 and coronaviruses, including SARS-CoV-2, bear similarities, from the presentation of a trimeric spike on both viral surfaces (glycoproteins gp41/gp120 and the S (spike) glycoprotein, respectively), to the recognition and binding of these viral spikes to ubiquitous cell surface structures, heparan sulfate proteoglycans (HSPGs).^[5] Epithelial cells, which dominate both the genitourinary tract and respiratory system, bear HSPGs which can be utilized by the viruses for initial attachment to the host cells, leading to viral fusion and infection. These binding events are mediated through electrostatic interactions between the polyanionic sulfate groups on the sugars coating the HSPGs and the solvent accessible polybasic amino acids on the surface of the viral spikes. In HIV-1, the dominant polybasic region is the variable V3 loop in gp120, characterized by the close proximity of multiple basic amino acids. This high density of positive charges is essential for viral infectivity and is conserved even though the V3 loop displays an increased level of mutation in different isolates.^[6] For SARS-CoV-2, preliminary data indicate the polybasic amino acids are contained within the receptor binding domain (RBD) of the Spike protein.^[7] For both HIV-1 and SARS-CoV-2, the binding interactions between the trimeric viral spikes and the host cell HSPGs have the potential of being multivalent, whereby multiple viral proteins/spikes can come into contact with multiple complementary host cell surfaces such as the HSPGs. Multivalent binding is commonly utilized in nature to increase binding affinity. This is particularly relevant when it comes to improving the binding strength of carbohydrates, which are typically very weak (mM– μ M dissociation constants) in 1:1 interactions, but can be improved by orders of magnitude (nM–pM) if the sugars are clustered on a surface or synthetic scaffold.^[8]

Considering the similarities in the trimeric viral surface proteins of HIV Env and the SARS-CoV-2 Spike, along with the mode of viral binding to the host cell surface HSPGs, we believe it is possible to develop antiviral agents that encompass properties that can be used to prevent the binding of both viruses to the host cell HSPGs. Inhibition of multiple pathogens by HSPG-mimicking dendrimers/glycodendrimers has been recently reviewed.^[9] These include surface-sulfated carbosilane dendrimers with demonstrated activities against HIV-1 and HSV-2 by the Muñoz-Fernández group, and VivaGel[®], which is a lysine-core naphthalene disulfonic acid derivatized dendrimer developed by Starpharma in Australia. Starpharma has licensed VivaGel[®] for use in limited countries for the treatment of bacterial vaginosis and as a condom formulation to prevent the transmission of sexually-transmitted pathogens, however, it is not approved for use in the United States.^[10] Further work is needed to develop broad-spectrum antiviral agents capable of reining in the transmission and morbidity/mortality associated with both HIV-1 and SARS-CoV-2, as these two viruses are responsible for pandemics currently gripping the world.

In the current study, multivalent sulfoglycodendrimers (SGDs) were designed to prevent the binding of the gp41/gp120 trimeric spike of HIV-1 to the HSPGs on the host cell surface. These molecules are made polyanionic through the incorpo-

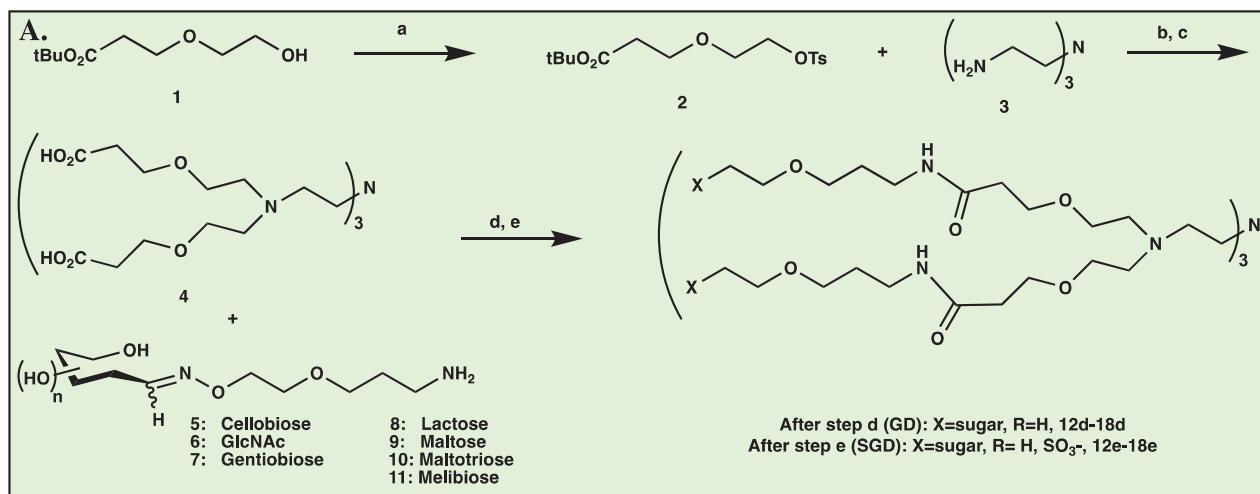
ration of multiple sulfated sugars on a multivalent dendrimer core structure. We previously showed that a large hexadecavalent sialic acid-terminated SGD, Sulfo-6, was able to bind to the V3 loop of gp120 and prevent HIV-1 infection through an HIV neutralization luciferase reporter gene assay.^[11] Sulfo-6 achieved an average IC₅₀ (inhibitory concentration for 50% inhibition) value in the neutralization assay of 3.3 μ M (over all 4 pseudoviruses tested), at a molecular weight of 8777 g mol⁻¹ and 4.03% sulfur (0.68 sulfates/sugar). In the present study, this strategy was further developed to yield more potent SGDs against HIV-1. To achieve this goal, we altered our synthetic strategy to reach the target compounds more efficiently and with significantly improved yields, while using common sugars. Here we hypothesized that we could obtain better biological activity in our next series of SGDs through decorating the surface of a smaller hexavalent dendrimer core with clusters of oligosaccharides, rather than using larger cores with single sugars appended. We also evaluated whether the type of sugars or glycosidic linkages incorporated were critical for the resultant biological activity. Here we utilized seven common sugars: cellobiose, *N*-acetylglucosamine (GlcNAc), gentiobiose, lactose, maltose, maltotriose, and melibiose.

The anti-HIV activity of the seven SGDs was assessed using a combination of techniques including: enzyme-linked immunosorbent assay (ELISA), microscale thermophoresis (MST), an HIV neutralization assay, and molecular dynamics calculations (MD). Additionally, in light of the emergent pandemic caused by SARS-CoV-2, two of our most promising anti-HIV SGDs were evaluated by MD to generate preliminary binding characteristics between the glycodendrimers and the open configuration of the RBD on the S spike. This allowed us to determine if the target SGDs have the potential to display antiviral activity against both SARS-CoV-2 and HIV-1. In this report, we demonstrate the potential of SGDs to serve as broadly active antiviral agents against pandemic-causing viruses. For HIV-1, these molecules can serve as topical microbicides and prevent the sexual transmission of the virus. There are currently no FDA-approved topical microbicides. For SARS-CoV-2, the potential exists for the application of SGDs through the nose or mouth to reduce the symptoms, morbidity, and mortality associated with COVID-19.

2. Results and Discussion

2.1. Synthesis

The synthesis of the desired SGDs is illustrated in **Figure 1A**. To begin, a water-soluble hexavalent poly(ether-amide) carboxy-terminated dendrimer was synthesized starting with 1,^[12] which was first tosylated, yielding 2^[13] in 95% isolated yield. Compound 2 was next combined in excess with tris(2-aminoethyl)amine (3) refluxing under basic conditions, providing the carboxyl-terminated hexavalent dendrimer, 4, in a 75% two-step yield after deprotection. Core 4 was subsequently amide-coupled with 2-(1H-Benzotriazole-1-yl)-1,1,3,3-tetramethylammonium tetrafluoroborate (TBTU) overnight at room temperature with seven different sugar linker molecules (Boc-deprotected, 5–11), prepared using a microwave-mediated oxime-forming reaction we reported previously,^[14] providing the target glycodendrimers (GDs,



B. General Structural Characteristics

| Compound: GD: X=12d-18d, R=H SGD: X=12e-18e, R=H, SO ₃ ⁻ | GD: % Yield | GD: MW (g/mol) | SGD: % Yield | SGD: Appx. MW (g/mol) | SGD: % Sulfur | SGD: Total # Sulfates (# sulfates/sugar) |
|--|----------------|-------------------|-----------------|--------------------------|------------------|--|
| Cellobiose, 12d,e | 85 | 3485 | 67 | 5061 | 12.6 | 20.0 (1.7/sugar) |
| GlcNAc, 13d,e | 46 | 2757 | 48 | 3484 | 8.7 | 9.0 (1.5/sugar) |
| Gentiobiose, 14d,e | 60 | 3485 | 82 | 4260 | 7.0 | 10.0 (0.8/sugar) |
| Lactose, 15d,e | 69 | 3485 | 64 | 5219 | 13.4 | 22.0 (1.8/sugar) |
| Maltose, 16d,e | 81 | 3485 | 64 | 4911 | 11.8 | 18.0 (1.5/sugar) |
| Maltotriose, 17d,e | 49 | 4456 | 74 | 6583 | 13.0 | 27.0 (1.5/sugar) |
| Melibiose, 18d,e | 57 | 3485 | 84 | 4826 | 11.2 | 17.0 (1.4/sugar) |

Figure 1. A) Synthesis of seven SGDs containing common mono, di, and trisaccharides. a) TsCl, pyridine, CH₂Cl₂, overnight, room temperature. b) K₂CO₃, acetonitrile, reflux, 48 h. c) TFA, CH₂Cl₂, room temperature, 2 h. d) TBTU, DIPEA, DMSO, pH = 9, overnight. e) SO₃-pyridine, DMF, 0 °C, 1 h. B) Summary of structural data for Compounds 12d,e–18d,e.

12d–18d) is in good to excellent yields after purification (46–85% isolated yields, Figure 1B). The sugar termini on GDs 12d–18d were finally sulfated, giving the seven target SGDs, 12e–18e (48–84% isolated yields, with % sulfur ranging from 7.0–13.4%, or 0.8–1.8 sulfate groups, per sugar, Figure 1B), after purification.

2.2. Anti-HIV Activity

To assess the potential anti-HIV activity, we undertook a 3-pronged assay approach. Our first assay is a simple competitive binding ELISA using a Ni²⁺-coated assay plate and binding (His)₆-tagged recombinant gp120 (rgp120) (Figure 2). The competition binding step utilized a constant amount of horseradish peroxidase (HRP) tagged V3 loop specific monoclonal antibody and varying amounts of SGD or the positive assay control, dextran sulfate (DS) (0.1–400 μg mL⁻¹). The endpoint absorbances were used to generate dose-response curves and determine the IC₅₀ values. The IC₅₀ values were used to determine whether or not the SGD had a binding affinity to the V3-loop of rgp120. Here we found that six of the seven SGDs were positive with IC₅₀ values ranging from 3.5–129.3 μM, with the Lactose-SGD, 15e, the best performer, and the Gentiobiose-SGD, 14e, the weakest. The GlcNAc-derivative (13e) was negative. We believe that GlcNAc was not positive because, with only a monosaccharide on the surface of the dendrimer core, it does not possess a large enough surface area/size to interact effectively with the V3 loop of gp120. This matches what we observed with our earlier SGDs. With a molecular mass of 3484 g mol⁻¹, it is 13% smaller than our octavalent SGD that was shown to be only weakly positive in our inhibition of infectivity assay, and is 22% larger than the tetravalent SGD that was negative for any anti-HIV activity.^[11a]

Moving forward with the six gp120-positive binding SGDs plus our positive control DS, we next assessed the solution binding properties using MST (Figure 3).^[15] These measurements allowed us to calculate quantitative dissociation constants (K_d) for binding to the monomeric rgp120. Here we performed an initial MST scan for each SGD at the two concentration extremes, 0 and 50 000 nmol, of the SGD. From this initial screen, it was determined that the gentiobiose-SGD, 14e, did not show a significant difference in the two MST signals, so it was not evaluated further by MST. This was anticipated given the weak binding noted in the ELISA. The remaining 5 SGDs, 12e, 15e–18e all gave significant dose response curves, yielding the K_d values shown in Figure 2. Similar to what was observed in the ELISA, the lactose SGD, 15e, gave the lowest K_d value of 0.6 μM. The order of binding from strongest to weakest SGDs was: Lactose(15e), Maltotriose(17e), Cellobiose(12e), Maltose(16e), Melibiose(18e).

The final assay used to assess the anti-HIV activity for all seven SGDs was an HIV neutralization luciferase reporter gene assay.^[11] This assay utilizes 4 HIV pseudoviruses (Q23.17, MN.3, MW965.26, and TV1.21) representing HIV clades A, B, C, and C, respectively, and TZM-bl cells displaying the HIV receptor CD4, and coreceptors, CXCR4 and CCR5, on the surface. The pseudoviruses are replication-defective, allowing only a single round of infection. For detection of infection events, the TZM-bl cells have been modified to contain the firefly luciferase gene that is under the control of an HIV promoter. In this assay, when a positive infection event occurs, the luciferase protein is produced, resulting in a chemiluminescent response. This response

is inversely proportional to the activity of the inhibitors that are added into the assay in a dose-response fashion. The more potent the inhibitor, the lower the resultant chemiluminescent signal. Much like what was observed for the ELISA, the GlcNAc-SGD, 13e, did not possess any measurable activity, while the Lactose-SGD, 15e, was again the strongest inhibitor (Figure 2). The six active SGDs all possessed micromolar to sub-micromolar (μM) activities, which is in line with the K_d values obtained by MST. This instills confidence that the observed antiviral activities against the pseudoviruses were due to binding between the SGDs and gp120. These activities compare well with those reported for other anti-HIV-1 dendrimers/glycodendrimers. Our compound 15e (5219 g mol⁻¹) possessed a range of IC₅₀ values (over 4 pseudovirus HIV-1 strains) of 0.34–0.42 μM. The sulfated carbosilane dendrimer, G2-S16 (3717 g mol⁻¹) gave a range of EC₅₀ values 6.2–31 nM across 3 different HIV-1 strains.^[16] For VivaGel® (SPL-7013, 16 582 g mol⁻¹), a range of EC₅₀ values of 0.05–0.26 μM was obtained for 11 different strains of HIV-1.^[17] For a glycodendrimer comparison, a 5th generation sulfated GalCer glycodendrimer with a polypropyleneimine core (18 261 g mol⁻¹, with 44 of 64 sites occupied by Gal) was reported by Schengrund and coworkers to have EC₅₀ values ranging from 0.6–100 nM across 4 different viral strains.^[18] It should be noted, however, that as the strains and assay methods utilized were not the same for the different inhibitors, a more direct comparison of inhibitor activities is not possible.

Beyond the anti-HIV activities, it was important to assess the cytotoxicity of the SGDs to ensure that they were not toxic to the cells. Using the same TZM-bl cells, it was determined that none of the SGDs caused cell death in the concentration range tested (up to a maximum of either 25 or 50 μg mL⁻¹), while our assay positive control, DS, was significantly cytotoxic, causing a 45% reduction in the cell population at a concentration of 50 nM (Figure 2, last column). DS is known to have potent *in vitro* anti-HIV activity, but with significant cytotoxicity and poor bioavailability.^[19] While the maximum compound concentrations assayed here are relatively low, our most potent inhibitor (15e, with sub-micromolar IC₅₀ values) was completely non-cytotoxic at a concentration >tenfold that of the IC₅₀s against all four HIV strains. Additional evaluation of cytotoxicity at higher concentrations will be needed to determine whether other compounds achieve a reasonable therapeutic index.

2.3. MD Simulations of SGD Binding Interactions with Trimeric HIV-1 gp120

To better understand how and where specifically the SGDs interact with the HIV-1 gp120 protein, we set out to evaluate the binding interactions of the four most active SGDs based on the inhibition of infectivity results (12e, 15e, 17e, and 18e). The average number of sulfates incorporated was 1.6/sugar (cellobiose, 12e), 1.8/sugar (lactose, 15e), 1.0/sugar (maltotriose, 17e), and 1.2/sugar (melibiose, 18e), which varies slightly from the experimental number. The DS was used as a positive control, while the four non-sulfated GDs were negative controls. All of the systems were immersed in 150 mM NaCl solutions. Figure 4 shows the two most favorable binding configurations of each SGD to the gp120 trimer (HIV spike proteins). All four of these SGDs are able to bind to the gp120 trimer in a multivalent

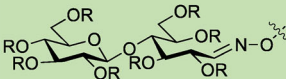
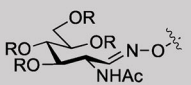
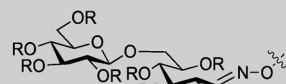
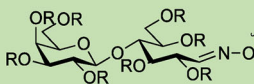
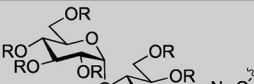
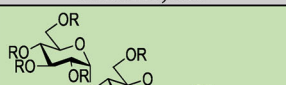

| Structures | Gp120 Binding Results | | Inhibition of Infectivity Results | | | | Toxicity Results |
|--|--|--|-----------------------------------|--|--|--|--|
| | Compound X=12e-18e R=H, SO ₃ ⁻ | ELISA IC ₅₀ ^a | MST K _d ^b | Q23.17 (Clade A) IC ₅₀ ^c | MN.3 (Clade B) IC ₅₀ ^c | MW965.26 (Clade C) IC ₅₀ ^c | TV1.21 (Clade C) IC ₅₀ ^c |
|  Cellobiose, 12e | 17.8 μM | 1.6 ± 0.5 μM | 1.2 μM | 0.51 μM | 0.52 μM | 0.69 μM | > 4.9 μM |
|  GlcNAc, 13e | >114.8 μM | NA | >7.2 μM | >7.2 μM | >7.2 μM | >7.2 μM | >7.2 μM |
|  Gentiobiose, 14e | 129.3 μM | NA | 9.7 μM | 1.6 μM | 9.5 μM | 7.9 μM | > 11.7 μM |
|  Lactose, 15e | 3.5 μM | 0.6 ± 0.2 μM | 0.42 μM | 0.35 μM | 0.38 μM | 0.34 μM | > 4.8 μM |
|  Maltose, 16e | 44.4 μM | 2.0 ± 0.3 μM | >10.2 μM | 2.9 μM | 8.4 μM | 3.4 μM | >10.2 μM |
|  Maltotriose, 17e | 9.5 μM | 0.8 ± 0.07 μM | 3.3 μM | 0.84 μM | 2.7 μM | 0.94 μM | >7.6 μM |
|  Melibiose, 18e | 6.2 μM | 2.6 ± 0.6 μM | 1.0 μM | 0.11 μM | 0.74 μM | 0.93 μM | >5.2 μM |
| DS | 0.8 nM | 1.0 ± 0.3 nM | 8.2 nM | 4.4 nM | 2.8 nM | 2.6 nM | 45% RLU (50 nM) |
| CHO1-31 | NA | NA | <0.07 nM | 4.8 nM | 17.3 nM | 10.4 nM | NA |

Figure 2. Summary of all biological data for SGDs, Compounds 12e–18e. General notations: NA, Assay not conducted. Colors: Green-Significant activity, Gray-No significant activity, Yellow-Positive assay controls. ^aELISA assays report the average IC₅₀ value obtained for a minimum of two assays for each compound and evaluated concentrations of 0–400 μg mL⁻¹ in duplicate wells. ^bMST K_d values were obtained from triplicate measurements of serial dilutions (0.01–50 000 nmol) of the SGDs evaluated. ^cEach sample concentration was tested in duplicate. For SGDs 12e–18e, the presence of a greater than (>) sign indicates that no reduction in the luciferase signal was observed at any concentration tested (0.02–50 μg mL⁻¹) compared to no test sample. For DS and CHO1-31, sample concentrations ranged from 0.01–25 μg mL⁻¹. ^dFor the cytotoxicity assessment, 12e–18e and DS were tested for reduction of relative luminescence units (RLU) after 48 h as compared to a no compound control. The concentrations presented are as follows: 0–50 μg mL⁻¹ for 14e, 16e and 17e and 0–25 μg mL⁻¹ for 12e, 13e, 15e, 18e, and DS, respectively. No measurable toxicity was observed for 12e–18e as evidenced by the > sign in front of the highest concentration tested, while for DS, a 45% drop in the living cell population was observed at 50 nM concentration, as measured by the presence of ATP.

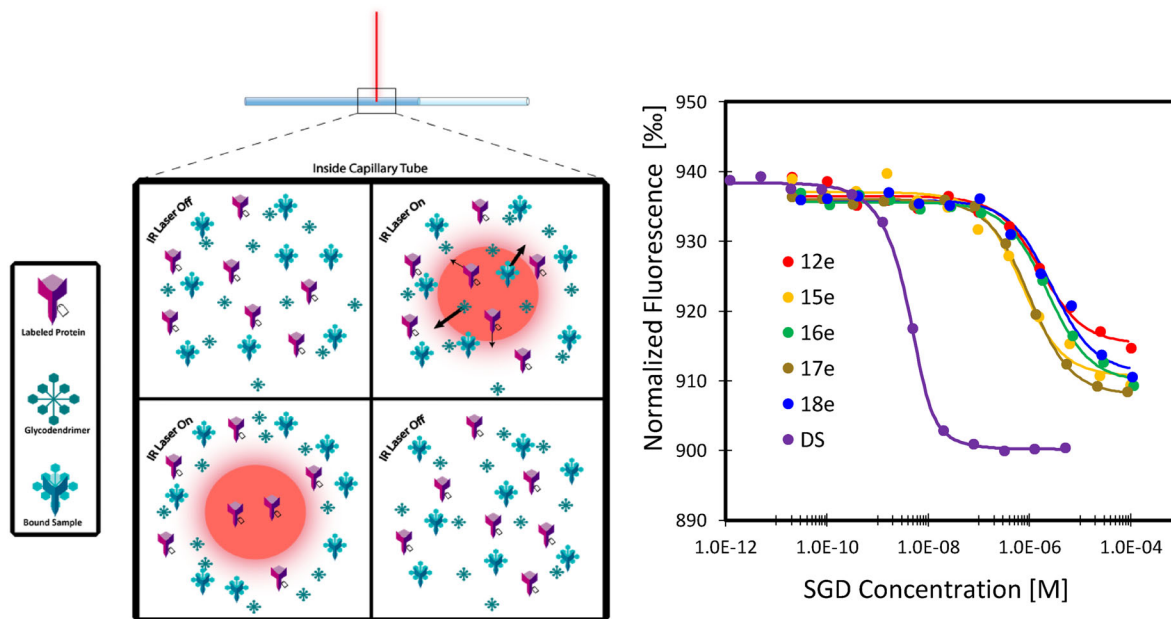


Figure 3. MST summary. Left panel: Diagram illustrating the general MST experiment process. At the top, a quartz capillary loaded with sample is heated with a laser focused on a narrow region of the capillary tube. Upper left quadrant: The initial random distribution of fluorescently-tagged protein in the bound and unbound states with the glycodendrimer at equilibrium. Upper right quadrant: Once the laser is turned on, the temperature gradient will cause the bound and unbound proteins to migrate out of the heated area at different rates. Lower left quadrant: This depicts the heated region of the capillary after the differential migration of the bound/unbound proteins. Lower right quadrant: The molecules return to a random distribution in the capillary after the laser is turned off. Right panel: MST results for selected SGDs plus positive control DS. The labeled-gp120 concentration is 200 nM for all trials, and the y-axis represents the MST responses at the 5 s mark after heating.

manner, where the different functional groups of the SGDs interact with gp120 in a correlated manner by the Coulombic and van der Waals (vdW) coupling.^[20] In this multivalent coupling, different branches of SGDs can simultaneously interact with one or two gp120 monomers, as shown in Figures 4B, Figure S40, Supporting Information, for the Lactose-SGD (15e) compound. On the other hand, the neutral GDs (non-sulfated, 12d, 15d, 17d, and 18d) are significantly less active in their binding with gp120 (Figures S41 and S42, Supporting Information).

The interacting amino acids were divided into three categories: positively charged, hydrophobic, and polar (polar uncharged and negatively charged). The percentage of each type of interaction with the four SGDs is shown in Figure 4E, obtained from the number of interaction times for each type of amino acid over the last 20 ns period (500 frames), divided by the overall contact times of all amino acids. Figures S43 and S44, Supporting Information, show the contact times of amino acids of the V3 loop interacting with different SGD/GDs. The contact time is defined as the number of frames out of the last 500 where the interaction or contact is apparent. Arg and Ile are frequent interacting amino acids, exemplifying the charged and hydrophobic classes of interactions with SGD/GDs. The interacting residues were selected either from the V3 loop or from the whole protein, as shown in Figure 4E. Because the V3 loop is a hyperbasic region on gp120, it is not surprising that charged interactions with the V3 loop are more than 10% higher than what was observed for the entire gp120 protein. The percentage of hydrophobic interactions are comparable for both Cellobiose and Lactose-SGDs (12e, 15e) in the two sets of analysis, and the percentage of polar interactions is complementary to that of the positively charged interactions in the two SGDs.

In our earlier studies of sulfonated gold NPs coupled with Human Papilloma Virus (HPV) capsids, we found that the free energy per one charged interaction (-6 kcal mol^{-1}) is 12 times larger than that per one typical hydrophobic group (alkyl, $-0.5 \text{ kcal mol}^{-1}$).^[20d] Coulombic coupling should also dominate the binding of SGDs and gp120. Furthermore, the ranking of SGDs in order of their charged interaction contribution (Figure 4E, left) matches their binding affinities obtained from MST experiments: $15e > 17e > 12e > 18e$. However, the ranking of SGDs sorted by sulfation level ($15e > 12e > 17e > 18e$) is slightly different from that of the experimental binding affinity (MST). The spatial orientations of hydroxy groups, the number of sugar units, and the linkage between sugar units are all contributing in a delicate manner to the overall strength of SGDs and gp120 binding. Lactose, with three hydroxy groups on one side of the ring structure and a β -1 \rightarrow 4 glycosidic linkage, could provide a more polar face, leading to stronger binding of 15e to gp120 (Figure S45, Supporting Information). We conclude that the sulfation level, number of sugars, orientations of polar groups, and overall arrangement of sugars in SGDs determine the strength of their multivalent interactions with target substrates.^[20a-d,21]

2.4. MD Simulations of SGD Binding Interactions with Monomeric SARS-CoV-2-S Spike

Due to the emergence of the COVID-19 pandemic caused by the SARS-CoV-2 virus, and the similarities shared between HIV-1 and coronaviruses in interacting with the ubiquitous cell surface

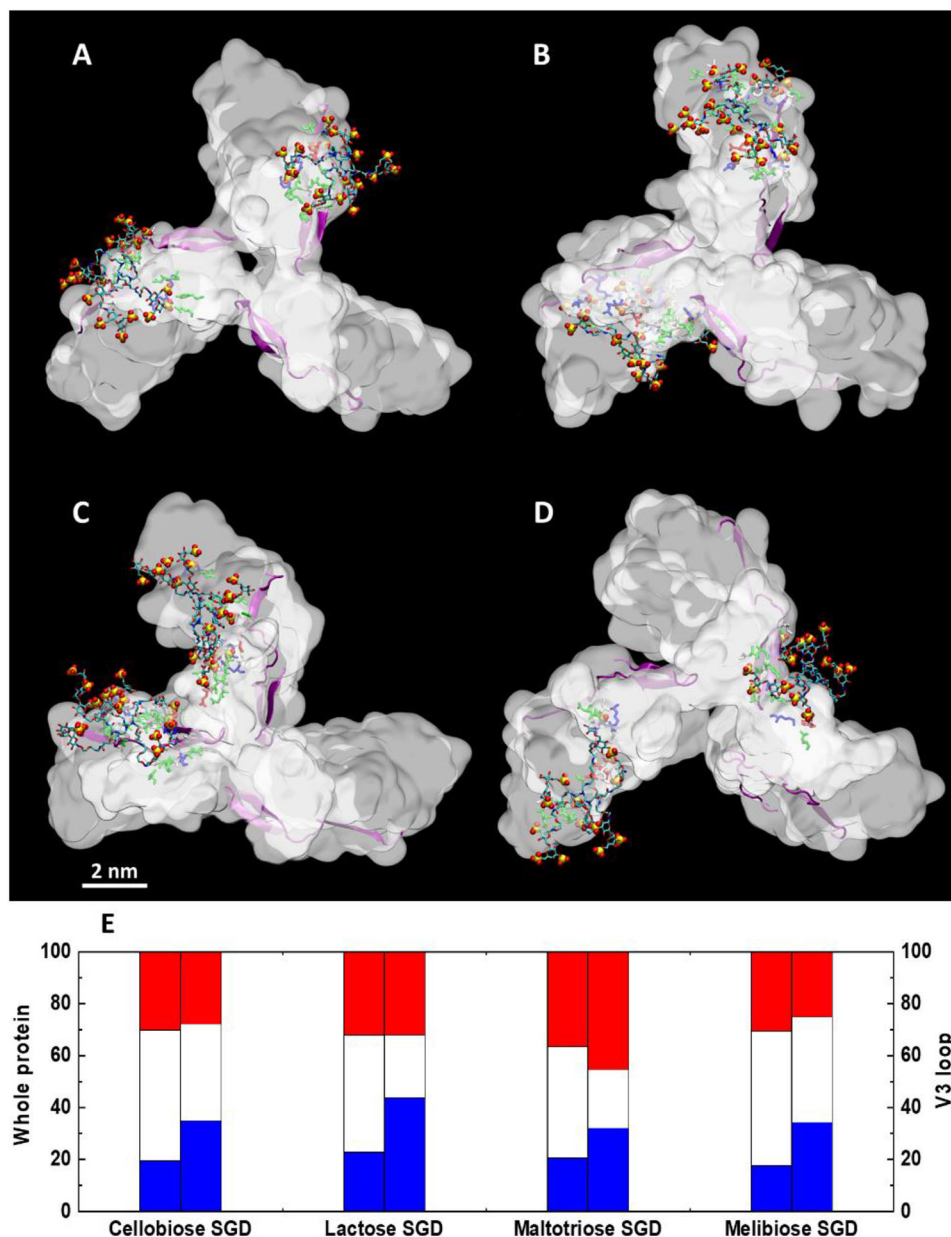


Figure 4. Different SGDs attached to one gp120 trimer: A) Cellobiose-SGD (12e); B) Lactose-SGD (15e); C) Maltotriose-SGD (17e); D) Melibiose-SGD (18e). Only two SGDs with the most favorable binding configurations are shown in each case. Proteins are shown as a white surface, SGDs are represented in atomistic details, and the gp120 residues interacting with SGDs (within 3 Å) are shown in licorice. The coloring scheme: V3 loop–purple; SGD atoms: C–cyan, O–red, S–yellow, N–blue, H–omitted; basic residue–blue, acidic residue–red, polar residue–green, nonpolar residue–white. Water and ions are omitted for better visualization. E) Percentage of different interactions contributing to the SGD-gp120 binding (left bar: quantified over the whole protein; right bar: quantified only with V3 loop). Polar–white: interaction with polar amino acids; hydrophobic–red: interaction with hydrophobic amino acids; charge–blue: interaction with positively charged amino acids.

proteoglycan, HSPG,^[7] we selected two of our best performing SGDs, Cellobiose 12e, and Lactose 15e, to determine how they interact with the RBD of SARS-CoV-2. Specifically, the type and locations of amino acids contacting the SGDs were identified. Cellobiose and Lactose GDs (12d and 15d) were selected as controls. As the basic amino acids concentrated in the middle part of RBD on the front side (HSPG binding),^[7] and the host cell receptor (ACE2) binding region resides on the top of RBD,^[7c,22]

the four compounds were initially placed near the top and middle regions of RBD, respectively. Two trials were conducted for each molecule. Our simulations show that the SGDs 12e and 15e can target either the top or the middle region of RBD separately, but not simultaneously (Figure 5A,B, and Figures S48 and S49, Supporting Information), while the GDs 12d and 15d only bind the top part of RBD due to the lack of sulfate groups (Table S2, Figures S49 and S50, Supporting Information). The

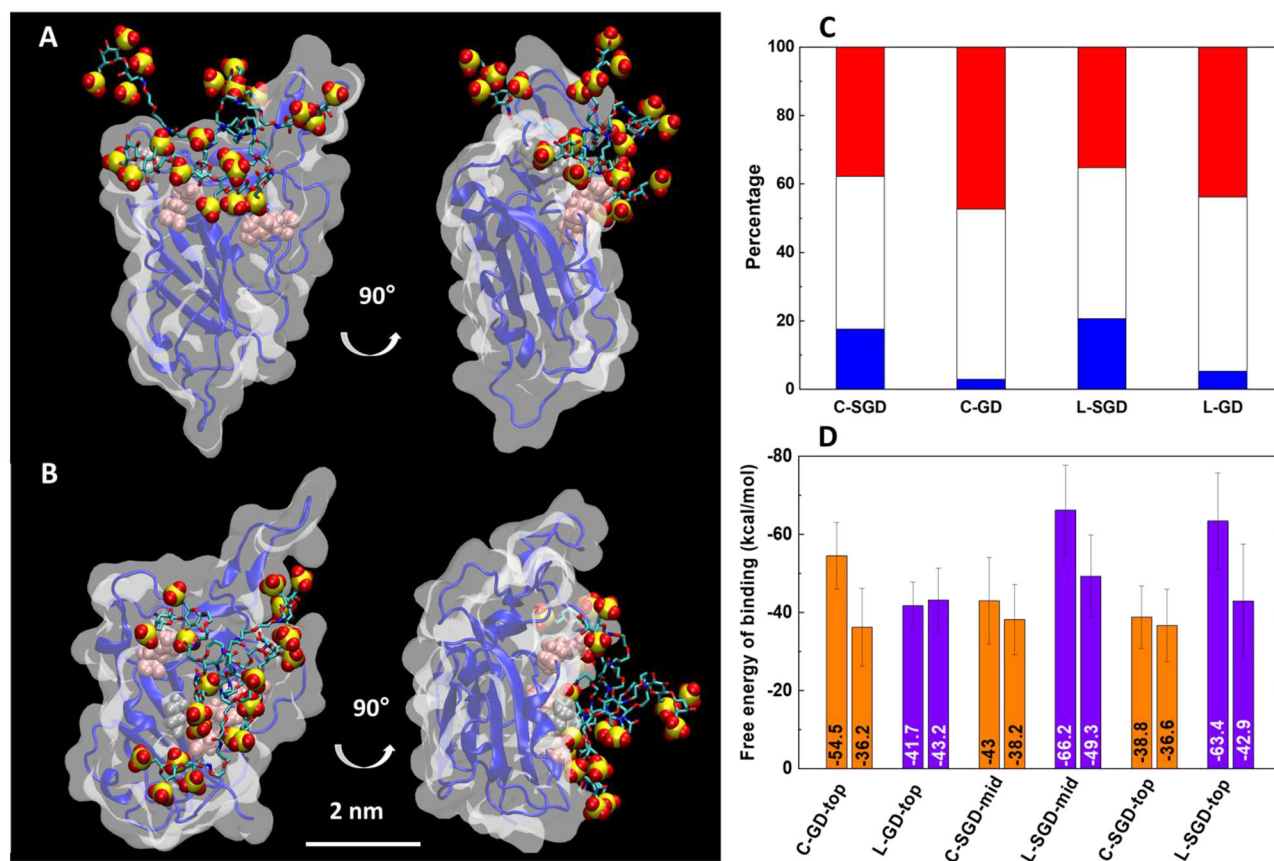


Figure 5. Lactose SGD (15e) binding with RBD of SARS-CoV-2. A) Two views (90° rotation) of 15e binding with the ACE2 binding region. B) Two views (90° rotation) of 15e binding with the purported HSPG binding region. Coloring scheme: SGD: C-cyan, O-red, S-yellow, N-blue, H-omitted, SARS-CoV-2 interacting amino acids: Arg-pink, Lys-grey. Water and ions are omitted for better visualization. C) Percentage of different interactions contributing to the binding to the RBD of SARS-CoV-2 averaged over all the binding modes. Polar-white: interaction with polar amino acids; hydrophobic-red: interaction with hydrophobic amino acids; charge-blue: interaction with positively charged amino acids. C-cellobiose (12e); L-lactose (15e). D) Free energy of binding for GDs (12d, 15d) and SGDs (12e, 15e) with RBD of SARS-CoV-2 (two trials for each system). Top: refers to the initial placement of the GD/SGD near the ACE2 binding region. Mid: Refers to the initial placement of the GD/SGD near the HSPG binding region.

two most favorable binding modes of 15e, targeting either the top or the middle region of RBD, are shown in Figure 5A and B, where the interacting Arg and Lys residues are highlighted. Most of the branches of 15e interact with the basic amino acids near the top of RBD. Branches of 15e could span the top region of RBD, which is facilitated by the charged interaction between the sulfate groups and basic amino acids, as shown in the side view of Figure 5A. Analogous to the gp120 systems, multiple ligands in SGDs develop multivalent binding to RBD. Moreover, 15e exhibits a stronger Coulombic coupling (percentage of charged interaction) and overall affinity to RBD than 12d, 12e, and 15d. (Figure 5C,D). As in the gp120 systems, charged interactions originating from sulfated groups largely dominate the SGDs' binding to RBD, the binding affinity of 15e with the highest sulfation level (3.6/branch) was expected to be larger than the others. Importantly, the SGDs and GDs with multiple binding modes to RBD were not designed to be specific inhibitors.^[7c] The flexibility of the branches of the dendrimers facilitates multivalent binding to the RBD, which causes different conformational changes to the RBD (Figure 5A, B and Figures S47–S53, Supporting Information). The SGDs could serve as broad-spectrum antivirals

against HIV, SARS-CoV-2, and other viruses utilizing HSPG as a receptor.

In order to design compounds targeting both the top and middle part of RBD simultaneously, the hybrid octavalent GDs (HGDs) were designed as conceptual compounds with both sulfated and non-sulfated ligands (Figure S51, Supporting Information). Figure S52, Supporting Information, shows the simulation for Cellobiose-HGD (C-HGD) with RBD and Figure S53, Supporting Information, is for Lactose-HGD (L-HGD) with RBD. The sulfation level is the same in C/L-HGD (3.0/branch). Although the octavalent HGDs have more ligand branches than the hexavalent SGDs, only four of their branches are sulfated, while all six branches are sulfated in SGD. Figure S55, Supporting Information, and Figure 5C (15e) show that the percentages of charged interactions are comparable in the cases of 15e, C-HGD, and L-HGD due to the compensation of non-sulfated ligands in HGDs. As discussed in the gp120 systems, charged interactions dominate the binding, the overall binding affinities of C/L-HGD are expected to be comparable to 15e (Figure S56, Supporting Information, and Figure 4D, respectively). Although the HGDs could not provide significantly higher binding affinity

than 15e, they can target both the top and middle parts of RBD simultaneously. HGDs could be promising inhibitors that target both the specific binding of ACE2 to the top of RBD and non-specific binding of HSPG to the middle of RBD.

3. Conclusion

Many viruses such as HIV-1 and the emerging SARS-CoV-2 utilize HSPGs in the initial stages of viral binding and infection. Herein we present the synthesis, biological and computational evaluation of a series of SGDs that, through these studies, show the significant potential of SGDs as broad-spectrum antiviral agents against both HIV-1 and SARS-CoV-2. The synthetic SGDs were designed as molecular mimics of HSPGs to prevent interactions between susceptible host cells and the virus and thwart infection. This could lead to early interventions for patients with known exposure to the virus, or to a decrease in the viral load and minimization of symptoms and illness duration for those displaying symptoms.

The biological evaluation of the SGDs against HIV-1 revealed a hierarchy of activities and the structural trends related to these activities. The clear winner across all biological assays was the Lactose-SGD (15e), with a molecular weight of 5219 g mol⁻¹, and the highest sulfate/sugar ratio (1.8), with an average IC₅₀ of 0.37 μM from the HIV neutralization assay. Compared to our previous report,^[11a] this represents a decrease in size of 41% compared to our best inhibitor, Sulfo-6, with a tenfold improvement in the average IC₅₀ value. Cellobiose-SGD (12e), Maltotriose-SGD (17e), and Melibiose (18e) were the next most active with sulfate/sugar ratios of 1.7, 1.5, and 1.4, respectively. At the bottom of the activity list were GlcNAc-SGD (13e) and Gentiobiose-SGD (14e). The low levels of biological activities seen here were likely due to the small overall size of the SGD, the monosaccharide substitution present for (13e), and a low sulfation ratio for 14e (0.8 sulfates/sugar). In general, the higher the % sulfation, the better the performance in the biological assays, across the board. However, in cases where similar levels of sulfation were present, more subtle structural features such as the number of sugars, identity of the sugar (glucose vs galactose), or the orientation of the glycosidic bond (α -1→4, α -1→6, β -1→4, β -1→6) appeared to influence the activity, which may explain why the ELISA, HIV neutralization and MST results differed for the SGDs with mid-range activities. However, this may also be a result of the differences in how the biological activities are measured in the techniques themselves. Interestingly, for the three SGDs with equivalent sulfation ratios, 13e, 16e, and 17e, the activity trend increases with increasing numbers of sugar terminal groups: monosaccharide, disaccharide, and trisaccharide, respectively. Another observation is that the Melibiose-SGD (18e), outperformed the Maltose-SGD (16e), even though they had similar sulfate/sugar ratios (1.4 and 1.5, respectively), again pointing to the subtler structural differences (galactose vs glucose on the non-reducing end and α -1→6 vs α -1→4 linkages, respectively).

From the MD simulations, we were able to observe more closely how the SGDs interacted with specific regions of both the trimeric gp120 in HIV-1 and the RBD of the Spike protein for SARS-CoV-2. This helps us to better understand the findings of the biological studies and guide further development of SGDs as broad-spectrum antiviral agents. The different binding

affinities (K_d) preserved by the SGDs are significantly driven by the sulfate/sugar ratios. Sulfate groups can increase the binding strength of SGD towards gp120 by Coulombic interaction, but it is the combination of different types of interactions that lead to the various efficiency of binding. Multivalency plays an important role in the strengthening of binding between protein-protein or inhibitor-protein interactions.^[20d,21,23] Here, the oxime-linked hexavalent scaffold provides the first level contribution to multivalency with additional contributions from the disaccharide or trisaccharide terminus. Orientations of hydroxyl groups and linkage between units are delicate factors determining the multivalency of the designed SGDs. For the HIV-V3 loop, the galactose terminus and β -1→4 linkage were found to be the most critical factors for the higher binding affinities. An optimization of the spatial structure of the SGD can be done by adjusting the number of sugar units, polar group orientation, and the glycosidic linkage, which is also essential for designing improved SGDs. In future studies, SGDs should be evaluated against SARS-CoV-2 using both MST and a SARS-CoV-2 neutralization assay. This can lead to the development of more potent inhibitors.

4. Experimental Section

General Methods: All chemicals were purchased from commercial sources and used without further purification. All solvents used were purchased dry (Dri-Solv) and utilized as is. Size exclusion chromatography (SEC) was carried out on a 2.5 × 120 cm Biogel P-10 column with 0.03 M NH₄HCO₃ running buffer on a Bio-Rad Biologic Duo Flow Chromatography system with a Quadtech detector, with monitoring at 214 and 225 nm. NMR data analysis and interpretation are addressed in the Supporting Information section.

(CO₂H)₆-Core (Compound 4): To a flame-dried round-bottomed flask, K₂CO₃ (331 mg, 2.4 mmol) was weighed. After placing the flask under N₂ (g), 10 mL of acetonitrile was added. Next, tris(2-aminoethyl)amine (Compound 3, 51.2 μL, 0.342 mmol) was added, followed by Compound 2 (825 mg, 2.4 mmol). The flask was fitted with a chilled condenser, and the reaction mixture was refluxed at 85 °C in an oil bath for 48 h. After 48 h, the flask was removed from the oil bath and the solution was filtered through Celite and rinsed with CHCl₃. The solution was evaporated under reduced pressure to yield a clear yellow oil. This oil was next dissolved in CHCl₃ and washed three times with 5% (w/v) NaHCO₃. The organic layer was washed with brine, then dried over anhydrous Na₂SO₄. Once dry, the organic layer was gravity filtered then evaporated under reduced pressure. The crude material was carried directly to deprotection in a 1:1 mixture of TFA:CH₂Cl₂ (5 mL each), which was stirred at room temperature under N₂ (g) for two hours, then evaporated under reduced pressure. The resultant oil was dissolved in 0.3M NH₄HCO₃ to neutralize the solution to approximately pH 6. The aqueous solution was washed with CHCl₃, then lyophilized. The crude, clear tan oil was finally purified by SEC, and the pooled fractions containing the desired product were lyophilized to yield a pale tan puffy solid, Compound 4 (217 mg, 75%). ¹H NMR (500 MHz, D₂O): δ 3.83 (t, 4H, J = 4.3 Hz), 3.73 (t, 4H, J = 5.8 Hz), 3.47 (t, 4H, J = 4.3 Hz), 3.37 (t, 2H, J = 6.7 Hz), 2.97 (t, 2H, J = 6.9 Hz), and 2.48 (t, 4H, J = 5.8 Hz). ¹³C NMR (125 MHz, D₂O, with an internal MeOH standard): δ 178.97, 67.50, 63.97, 52.91, 50.95, 47.18, and 36.59. High resolution electrospray mass spectrometry (HR-ESI⁺-MS) [M+Na]⁺ (C₃₆H₆₆N₄NaO₁₈) calc m/z = 865.4270. Found m/z = 865.4262.

General Procedure for the Deprotection of the Sugar-Linkers (5–11): Boc-protected Compounds 5–11^[14] (1 equiv.) were weighed into an oven dried flask and placed under nitrogen. Next, a mixture of TFA and CH₂Cl₂ was added and the reaction mixture was stirred at room temperature for 2 h before being evaporated under reduced pressure. The residue was resuspended in water/0.03M NH₄HCO₃ and lyophilized.

Compound 5: Starting with the Boc-protected derivative (117.5 mg, 0.211 mmol),^[14] and 1.5 mL each of CH₂Cl₂, and TFA were combined. Compound 5, a white, puffy amorphous solid resulted (103.4 mg (TFA salt), 0.181 mmol, 86%). ¹H NMR (500 MHz, D₂O): δ 7.70 (d, 0.3H, *J* = 5.4 Hz, E isomer), 7.01 (d, 0.1H, *J* = 5.6 Hz, Z isomer), 5.23 (d, 0.2H, *J* = 3.8 Hz), 4.67 (d, 0.2H, *J* = 8.0 Hz), 4.60 (t, 0.3H, *J* = 6.7 Hz), 4.56 (d, 0.3H, *J* = 7.9 Hz), 4.51 (d, 0.7H, *J* = 7.9 Hz), 4.31 (d, 0.2H, *J* = 9.2 Hz), 4.24 (m, 1.4H), 4.00–3.87 (m, 3.8H), 3.84–3.71 (m, 4.4H), 3.68 (m, 2.4H), 3.65–3.57 (m, 1.7H), 3.50 (m, 1.8H), 3.43 (m, 1.5H), 3.36–3.27 (m, 1.3H), 3.12 (t, 2H, *J* = 7.1 Hz), and 1.97 (m, 2H). ¹³C NMR (125 MHz, D₂O with internal MeOH std.): δ 153.24, 152.23, 103.19, 102.86, 102.84, 102.80, 96.06, 92.12, 90.29, 80.58, 79.08, 78.94, 78.74, 78.42, 76.31, 76.25, 76.10, 75.87, 75.81, 75.59, 75.09, 74.60, 74.20, 73.68, 73.63, 73.57, 73.47, 73.38, 72.92, 71.84, 71.64, 71.54, 71.41, 71.38, 70.66, 70.40, 69.78, 69.69, 69.64, 69.60, 69.32, 69.07, 68.81, 68.74, 68.68, 68.65, 68.33, 66.62, 62.36, 62.18, 60.91, 60.78, 60.45, 60.36, 60.24, 37.96, and 26.79.

Compound 6: Starting with the Boc-protected derivative (52.8 mg, 0.121 mmol),^[14] and 4.0 mL of CH₂Cl₂ and 1.5 mL of TFA were combined. Compound 6, a white, puffy amorphous solid resulted (54.6 mg, 0.121 mmol, quantitative). ¹H NMR (500 MHz, D₂O): δ 7.55 (d, 0.2H, *J* = 6.2 Hz, E isomer), 6.86 (d, 0.1H, *J* = 6.6 Hz, Z isomer), 4.71 (t, 0.3H, *J* = 7.2 Hz), 4.36 (d, 0.2H, *J* = 9.8 Hz), 4.31 (m, 0.3H), 4.26 (m, 1H), 4.10 (m, 0.4H), 3.85 (m, 1.2H), 3.79 (m, 2.3H), 3.69 (m, 2.7H), 3.64 (m, 0.8H), 3.56 (m, 0.5H), 3.13 (p, 2H, *J* = 6.5, 12.2 Hz), 2.08 (m, 2H), and 1.98 (m, 2H). ¹³C NMR (125 MHz, D₂O with internal MeOH std.): δ 174.78, 174.53, 174.17, 150.07, 149.74, 94.98, 90.89, 88.79, 77.21, 75.99, 74.93, 74.02, 73.95, 73.24, 73.18, 72.70, 71.60, 71.26, 70.93, 70.73, 70.08, 69.90, 69.71, 69.42, 69.31, 69.05, 68.88, 68.84, 68.78, 68.59, 68.49, 68.42, 68.37, 68.18, 67.99, 62.87, 62.75, 60.85, 60.79, 60.63, 60.38, 56.75, 54.15, 52.01, 51.70, 37.71, 37.55, 26.53, 22.21, 22.01, 21.94, and 21.14.

Compound 7: Starting with the Boc-protected derivative (319.4 mg, 0.572 mmol),^[14] 4.5 mL of CH₂Cl₂, and 1.5 mL of TFA were combined. Compound 7, an off-white, puffy amorphous solid resulted (327 mg (TFA salt), 0.572 mmol, quantitative). ¹H NMR (500 MHz, D₂O): δ 7.58 (d, 0.6H, *J* = 6.5 Hz, E isomer), 6.92 (d, 0.1H, *J* = 6.3 Hz, Z isomer), 4.96 (t, 0.2H, *J* = 6.3 Hz), 4.49 (m, 1H), 4.42 (t, 0.6H, *J* = 6.7 Hz), 4.42 (m, 1.6H), 4.13 (m, 1H), 3.97–3.84 (m, 3H), 3.81–3.65 (m, 7H), 3.48 (m, 2.4H), 3.39 (m, 1H), 3.31 (m, 1H), 3.11 (t, 2H, *J* = 6.9 Hz), and 1.95 (p, 2H, *J* = 6.2, 13.0 Hz). ¹³C NMR (125 MHz, D₂O with internal MeOH std.): δ 152.47, 151.52, 102.95, 102.86, 102.69, 90.29, 76.72, 76.12, 75.92, 75.67, 73.31, 73.24, 73.13, 73.04, 72.69, 71.40, 70.89, 70.25, 69.76, 69.72, 69.64, 69.40, 69.27, 69.00, 68.77, 68.56, 68.41, 68.36, 66.33, 60.75, 37.82, 37.71, 37.65, and 26.51.

Compound 8: Starting with the Boc-protected derivative (289.4 mg, 0.519 mmol),^[14] 4.5 mL of CH₂Cl₂, and 1.5 mL of TFA were combined. Compound 8, a yellowish, amorphous solid resulted (297 mg (TFA salt), 0.519 mmol, quantitative). ¹H NMR (500 MHz, D₂O): δ 7.68 (d, 0.5H, *J* = 5.4 Hz, E isomer), 6.99 (d, 0.1H, *J* = 5.4 Hz, Z isomer), 4.58 (t, 0.5H, *J* = 5.9 Hz), 4.48 (d, 0.5H, *J* = 7.8 Hz), 4.43 (d, 0.3H, *J* = 7.8 Hz), 4.29 (d, 0.2H, *J* = 9.3 Hz), 4.26 (d, 0.3H, *J* = 2.8 Hz), 4.23 (m, 1H), 3.96–3.87 (m, 4H), 3.83 (m, 1H), 3.82–3.62 (m, 10H), 3.53 (m, 1.5H), 3.09 (t, 2H, *J* = 6.4 Hz), and 1.94 (p, 2H, *J* = 6.1, 12.9 Hz). ¹³C NMR (125 MHz, D₂O with internal MeOH std.): δ 152.38, 103.72, 103.31, 103.20, 96.05, 90.29, 78.62, 78.51, 78.44, 76.32, 75.66, 75.39, 75.10, 74.67, 74.11, 73.56, 72.89, 72.82, 71.72, 71.45, 71.39, 71.33, 71.26, 69.72, 69.51, 69.06, 68.86, 68.82, 68.69, 68.64, 64.16, 62.33, 61.36, 61.21, 60.47, 60.39, 38.05, 37.97, and 26.77.

Compound 9: Starting with the Boc-protected derivative (293.3 mg, 0.526 mmol),^[14] 4.5 mL of CH₂Cl₂, and 1.5 mL of TFA were combined. Compound 9, yellowish amorphous solid resulted (300.7 mg (TFA salt), 0.526 mmol, quantitative). ¹H NMR (500 MHz, D₂O): δ 7.60 (d, 0.5H, *J* = 5.9 Hz, E isomer), 6.96 (d, 0.1H, *J* = 5.6 Hz, Z isomer), 5.41 (d, 0.4H, *J* = 3.7 Hz), 5.13 (two doublets, 0.6H, *J* = 3.9 Hz for both), 4.97 (m, 0.1H), 4.53 (t, 0.4H, *J* = 5.5 Hz), 4.28 (m, 1.5H), 4.13 (app t, 0.2H, *J* = 5.2 Hz), 4.01–3.91 (m, 2.2H), 3.88–3.64 (m, 11.4H), 3.59 (m, 1.8H), 3.42 (m, 1.3H), 3.11 (br app t, 2H, *J* = 6.4 Hz), and 1.96 (app t, 2H, *J* = 6.4 Hz). ¹³C NMR (125 MHz, D₂O with internal MeOH std.): δ 152.05, 100.72, 99.86, 90.30, 81.39, 80.47, 77.51, 76.84, 76.06, 73.79, 73.57, 73.37, 73.14, 73.06, 72.98,

72.94, 72.78, 72.35, 71.95, 69.68, 69.65, 69.62, 69.55, 69.32, 69.05, 68.80, 68.68, 68.64, 62.58, 62.37, 61.13, 60.79, 60.62, 38.05, 37.95, and 26.77.

Compound 10: Starting with the Boc-protected derivative (382.9 mg, 0.531 mmol),^[14] 4.5 mL of CH₂Cl₂, and 1.5 mL of TFA were combined. Compound 10, a yellowish amorphous solid resulted (390 mg (TFA salt), 0.531 mmol, quantitative). ¹H NMR (500 MHz, D₂O): δ 7.61 (d, 0.4H, *J* = 6.0 Hz, E isomer), 6.97 (d, 0.1H, *J* = 5.6 Hz, Z isomer), 5.41 (m, 1.3H), 5.15 (d, 0.1H, *J* = 4.0 Hz), 5.12 (d, 0.4H, *J* = 4.0 Hz), 4.54 (t, 0.5H, *J* = 5.4 Hz), 4.30 (d, 0.4H, *J* = 9.3 Hz), 4.25 (m, 1H), 4.00 (m, 2.3H), 3.94 (m, 1.2H), 3.91–3.76 (m, 8.2H), 3.75–3.65 (m, 6.4H), 3.64–3.58 (m, 3H), 3.42 (m, 1.3H), 3.12 (t, 2H, *J* = 6.3 Hz), and 1.96 (p, 2H, *J* = 5.9, 12.8 Hz). ¹³C NMR (125 MHz, D₂O with internal MeOH std.): δ 153.38, 151.83, 100.37, 100.00, 99.95, 90.18, 81.28, 80.42, 77.29, 77.11, 75.88, 73.46, 73.36, 73.05, 72.85, 72.73, 72.35, 72.22, 71.93, 71.59, 71.37, 71.16, 69.47, 69.15, 68.90, 68.64, 68.51, 62.38, 60.90, 60.63, 60.46, 37.92, 37.82, and 26.61.

Compound 11: Starting with the Boc-protected derivative (275.9 mg, 0.494 mmol),^[14] 4.5 mL of CH₂Cl₂, and 1.5 mL of TFA were combined. Compound 11, an amorphous off-white solid resulted (282.6 mg (TFA salt), 0.494 mmol, quantitative). ¹H NMR (500 MHz, D₂O): δ 7.57 (d, 0.5H, *J* = 6.5 Hz), 6.92 (d, 0.1H, *J* = 6.4 Hz), 4.96 (app d, 1H, *J* = 3.5 Hz), 4.64 (d, 0.1H, *J* = 8.0 Hz), 4.40 (t, 0.5H, *J* = 6.8 Hz), 4.27 (m, 0.3H), 4.22 (m, 1H), 3.97–3.80 (m, 7H), 3.73 (m, 4H), 3.65 (m, 4H), 3.09 (t, 2H, *J* = 6.8 Hz), and 1.93 (p, 2H, *J* = 6.1, 13.1 Hz). ¹³C NMR (125 MHz, D₂O with internal MeOH std.): δ 152.82, 151.74, 98.49, 98.35, 98.30, 98.27, 98.25, 92.36, 90.69, 77.13, 76.08, 75.86, 74.49, 74.26, 73.51, 73.18, 73.15, 72.83, 71.70, 71.61, 71.08, 70.95, 70.63, 70.43, 70.29, 70.24, 69.92, 69.74, 69.67, 69.61, 69.57, 69.46, 69.44, 69.09, 68.89, 68.78, 68.69, 68.64, 68.60, 68.54, 68.49, 68.38, 68.15, 66.66, 66.07, 65.94, 61.33, 61.27, 60.52, 37.96, 37.86, 37.79, 37.71, 26.68, and 26.64.

General Procedure for the Formation of (Sugar)₆-GDs (12d–18d): Compound 4 was first prepared as a 100 mg mL⁻¹ solution in methanol. Following this, the volume providing 1.0 equiv. was transferred to an oven-dried pear-shaped flask and evaporated under reduced pressure. Similarly, the sugar-linkers (5–11) was prepared as a 100 mg mL⁻¹ solution in water. The volume providing an excess (6.6–6.8 equiv.) of 5–11 was transferred to the flask containing 4, and the solution was next freeze-dried overnight. Next, 14.4 equiv. of TBTU was added to the flask, which was then placed under N₂ (g). Following this, 1–2 mL of DriSolv dimethyl sulfoxide (DMSO) was added. Finally, the pH was adjusted to ≈9–10 with DIPEA (*N,N*-diisopropylethylamine). The reaction mixture was stirred at room temperature for 24–30 h, before water was added and the solution was repeatedly freeze-dried to remove the DMSO. The resultant crude oil was purified first by dialysis against water in 2000 molecular weight cut-off (MWCO) dialysis tubing (Spectrum). The water was changed 3 times over 3.5 h, then the solution inside the dialysis tubing was freeze-dried. Finally, the oily solids were purified by FPLC. The resultant peaks were pooled separately, freeze-dried, and the GDs (12d–18d) were identified by NMR and confirmed by Matrix-Assisted Laser Desorption Ionization (MALDI) mass spectrometry.

(Cellobiose)₆-GD (Compound 12d): Compound 4 (14.9 mg, 0.0177 mmol), 5 (68.8 mg, 0.120 mmol), TBTU (81.8 mg, 0.255 mmol), DIPEA (pH ≈9–10), and DMSO (1 mL) were utilized. 52.1 mg (0.0150 mmol, 85%) of a white fluffy solid resulted after purification. ¹H NMR (500 MHz, D₂O): δ 7.68 (d, 1H, *J* = 5.5 Hz, E isomer), 7.00 (d, 0.2H, *J* = 5.5 Hz, Z isomer), 4.58 (t, 1H, *J* = 6.1 Hz), 4.54 (d, 1H, *J* = 7.9 Hz), 4.50 (d, 1H, *J* = 7.9 Hz), 4.30 (d, 0.6H, *J* = 9.2 Hz), 4.23 (app t, 2.4H, *J* = 4.0 Hz), 3.98–3.85 (m, 7.5H), 3.76–3.68 (m, 13H), 3.64–3.56 (m, 11H), 3.49 (m, 2.6H), 3.41 (m, 3.5H), 3.33 (t, 2H, *J* = 8.8 Hz), 3.26 (t, 4H, *J* = 6.7 Hz), 2.75 (br s, 5H), 2.65 (br app d, 5H), 2.51 (t, 4H, *J* = 5.8 Hz), and 1.79 (app t, 4H, *J* = 6.6 Hz). ¹³C NMR (125 MHz, D₂O with internal MeOH std.): δ 173.92, 152.04, 102.69, 90.27, 78.60, 78.38, 76.16, 75.97, 75.75, 75.68, 75.44, 73.50, 73.33, 72.79, 72.55, 71.61, 71.30, 69.62, 69.50, 68.90, 68.74, 68.61, 68.55, 68.49, 68.23, 66.94, 66.73, 62.25, 62.07, 60.75, 60.64, 60.28, 53.13, 51.41, 51.04, 36.58, 36.33, and 28.50. MALDI-MS [M+H]⁺ (C₁₃₈H₂₅₉N₁₆O₈₄) calc *m/z* = 3484.64815. Found *m/z* = 3484.64774.

(GlcNAc)₆-GD (Compound 13d): Compound 4 (14.4 mg, 0.0171 mmol), 6 (52.4 mg, 0.116 mmol), TBTU (79.9 mg, 0.246 mmol), DIPEA (pH ≈9–10), and DMSO (1 mL) were utilized. 21.5 mg (0.0078 mmol,

46%) of an off-white solid resulted after purification. ^1H NMR (500 MHz, D_2O): δ 7.51 (d, 0.8H, J = 6.2 Hz, E isomer), 6.83 (d, 0.2H, J = 6.6 Hz, Z isomer), 5.10 (t, 0.2H, J = 6.8 Hz), 4.68 (t, 0.7H, J = 7.0 Hz), 4.33 (m, 0.8H), 4.26 (m, 0.7H), 4.21 (m, 2.4H), 4.10 (m, 0.4H), 4.06 (m, 0.8H), 3.81 (m, 1.7H), 3.73 (m, 10H), 3.63–3.53 (m, 12H), 3.24 (m, 4H), 2.73 (br s, 4.6H), 2.64 (br app d, 5H), 2.48 (t, 4H, J = 5.8 Hz), 2.12 (s, 0.7H), 2.03 (m, 4H), and 1.77 (app q, 4H, J = 7.0, 13.9 Hz). ^{13}C NMR (125 MHz, D_2O with internal MeOH std.): δ 173.90, 150.63, 149.76, 74.87, 73.88, 72.82, 71.62, 71.10, 70.24, 69.48, 68.73, 68.61, 68.43, 68.26, 66.95, 63.04, 60.56, 53.13, 52.08, 51.44, 51.07, 36.58, 36.34, 28.53, 22.30, and 22.16. MALDI-MS $[\text{M}+\text{H}]^+$ ($\text{C}_{114}\text{H}_{217}\text{N}_{22}\text{O}_{54}$) calc m/z = 2758.49037. Found m/z = 2758.49734.

(Gentiobiose) $_6$ -GD (Compound 14d): Compound 4 (15.0 mg, 0.0178 mmol), 7 (69.0 mg, 0.121 mmol), TBTU (82.4 mg, 0.256 mmol), DIPEA ($\text{pH}\approx 9$ –10), and DMSO (1 mL) were utilized. 36.9 mg (0.0106 mmol, 60%) of a yellowish amorphous solid resulted after purification. ^1H NMR (500 MHz, D_2O): δ 7.58 (d, 0.9H, J = 6.4 Hz, E isomer), 6.94 (d, 0.2H, J = 6.2 Hz, Z isomer), 4.99 (t, 0.2H), 4.50 (d, 2H, J = 8.0 Hz), 4.42 (t, 1.2H, J = 6.8 Hz), 4.25 (m, 3H), 4.15 (m, 1.3H), 3.97–3.91 (m 5H), 3.80–3.67 (m, 14H), 3.59 (br app t, 10H, J = 5.7 Hz), 3.52–3.45 (m, 5H), 2.41 (t, 2.4H, J = 9.4 Hz), 3.32 (t, 2H, J = 8.9 Hz), 3.26 (t, 4.4H, J = 6.5 Hz), 2.75–2.65 (m, 9.4H), 2.51 (br app s, 5H), and 1.79 (br app t, J = 6.4 Hz). ^{13}C NMR (125 MHz, D_2O with internal MeOH std.): δ 173.98, 152.72, 151.64, 103.08, 90.61, 76.13, 75.88, 75.79, 73.44, 73.38, 73.34, 72.90, 71.68, 71.11, 70.47, 70.05, 69.98, 69.92, 69.82, 69.64, 68.93, 68.79, 68.67, 68.59, 68.51, 68.33, 67.01, 60.97, 53.21, 51.51, 51.14, 36.65, 36.41, and 28.56. MALDI-MS $[\text{M}+\text{H}]^+$ ($\text{C}_{138}\text{H}_{259}\text{N}_{16}\text{O}_{84}$) calc m/z = 3484.64815. Found m/z = 3488.937.

(Lactose) $_6$ -GD (Compound 15d): Compound 4 (11.0 mg, 0.0131 mmol), 8 (50.8 mg, 0.089 mmol), TBTU (60.4 mg, 0.188 mmol), DIPEA ($\text{pH}\approx 9$ –10), and DMSO (1 mL) were utilized. 31.3 mg (0.0090 mmol, 69%) of an off-white fluffy solid resulted after purification. ^1H NMR (500 MHz, D_2O): δ 7.68 (d, 0.7H, J = 5.6 Hz, E isomer), 7.00 (d, 0.1H, J = 6.0 Hz, Z isomer), 4.59 (t, 0.8H, J = 6.1 Hz), 4.54 (d, 0.2H, J = 7.8 Hz), 4.50 (d, 0.8H, J = 7.8 Hz), 4.45 (d, 0.5H, J = 7.8 Hz), 4.31 (d, 0.4H, J = 9.2 Hz), 4.24 (m, 2H), 4.15 (m, 0.5H), 4.09–3.86 (m, 7H), 3.82–3.63 (m, 18.6H), 3.61–3.53 (m, 11.7H), 3.26 (t, 4H, J = 6.6 Hz), 2.74 (br s, 5H), 2.64 (br app d, 5H), 2.51 (t, 4H, J = 5.5 Hz), and 1.79 (app t, 4H, J = 6.3 Hz). ^{13}C NMR (125 MHz, D_2O with internal MeOH std.): δ 174.03, 152.27, 103.31, 103.17, 90.37, 78.56, 78.37, 76.27, 75.61, 75.48, 75.32, 73.60, 73.33, 72.88, 72.81, 71.71, 71.56, 71.42, 71.30, 71.21, 70.63, 69.63, 69.53, 69.41, 69.01, 68.82, 68.76, 68.70, 68.64, 68.59, 68.52, 68.34, 67.04, 66.83, 66.72, 62.34, 62.14, 61.29, 61.13, 61.05, 60.65, 60.42, 53.22, 51.52, 51.16, 36.67, 36.42, 28.61, and 28.58. MALDI-MS $[\text{M}+\text{H}]^+$ ($\text{C}_{138}\text{H}_{259}\text{N}_{16}\text{O}_{84}$) calc m/z = 3484.64815. Found m/z = 3484.6450.

(Maltose) $_6$ -GD (Compound 16d): Compound 4 (17.5 mg, 0.0208 mmol), 9 (82.3 mg, 0.144 mmol), TBTU (97.1 mg, 0.302 mmol), DIPEA ($\text{pH}\approx 9$ –10), and DMSO (2 mL) were utilized. 58.5 mg (0.0168 mmol, 81%) of a white fluffy solid resulted after purification. ^1H NMR (500 MHz, D_2O): δ 7.57 (d, 0.6H, J = 6.0 Hz, E isomer), 6.94 (d, 0.1H, J = 5.6 Hz, Z isomer), 5.37 (d, 0.6H, J = 3.7 Hz), 5.09 (m, 0.8H), 4.50 (t, 0.6H, J = 5.7 Hz), 4.24 (m, 2.4H), 3.96 (m, 1.5H), 3.90 (m, 2H), 3.85–3.80 (m, 4H), 3.79–3.66 (m, 17H), 3.64–3.54 (m, 14H), 3.39 (m, 2.3H), 3.24 (br t, 4H, J = 6.7 Hz), 2.77 (br app d, 9H), 2.49 (br app s, 4H), and 1.77 (br app t, 4H, J = 6.3 Hz). ^{13}C NMR (125 MHz, D_2O with internal MeOH std.): δ 174.00, 160.58, 151.99, 100.88, 100.73, 99.97, 90.42, 80.54, 77.49, 76.09, 73.65, 73.38, 73.27, 73.18, 73.09, 73.00, 72.97, 72.78, 72.55, 72.44, 71.98, 71.75, 69.68, 69.63, 69.55, 69.04, 68.88, 68.76, 68.63, 68.57, 68.01, 67.10, 65.97, 62.61, 61.12, 60.80, 60.68, 53.44, 53.16, 51.21, 36.74, 36.43, and 28.67. MALDI-MS $[\text{M}+\text{H}]^+$ ($\text{C}_{138}\text{H}_{259}\text{N}_{16}\text{O}_{84}$) calc m/z = 3484.64815. Found m/z = 3488.011.

(Maltotriose) $_6$ -GD (Compound 17d): Compound 4 (17.5 mg, 0.0208 mmol), 10 (99.1 mg, 0.135 mmol), TBTU (96.1 mg, 0.299 mmol), DIPEA ($\text{pH}\approx 9$ –10), and DMSO (2 mL) were utilized. 45.8 mg (0.0103 mmol, 49%) of a white fluffy solid resulted after purification. ^1H NMR (500 MHz, D_2O): δ 7.61 (d, 1H, J = 6 Hz, E isomer), 6.98 (d, 0.2H, J = 5.5 Hz, Z isomer), 5.41 (dd, 2.3H, J = 3.8, 9.2 Hz), 5.14 (d, 1.2H, J = 4.0 Hz), 4.54 (t, 1H, J = 5.5 Hz), 4.32–4.25 (m, 3H),

4.02–3.98 (m, 4.4H), 3.95 (m, 2.2H), 3.90–3.84 (m, 7.6H), 3.82–3.66 (m, 21H), 3.65–3.58 (m, 13H), 3.43 (t, 2H, J = 9.4 Hz), 3.28 (m, 4H), 2.78 (br app s, 4H), 2.68 (br app d, 4H), 2.52 (t, 4H, J = 5.7 Hz), and 1.81 (app t, 4H, J = 6.5 Hz). ^{13}C NMR (125 MHz, D_2O with internal MeOH std.): δ 173.90, 151.92, 100.44, 100.03, 99.97, 99.79, 90.33, 80.52, 77.36, 77.19, 77.09, 77.03, 75.97, 73.57, 73.44, 73.29, 73.11, 72.92, 72.84, 72.46, 72.35, 71.97, 71.68, 71.42, 71.21, 69.60, 69.53, 69.49, 68.95, 68.80, 68.68, 68.55, 67.75, 67.03, 65.92, 62.48, 60.69, 53.03, 36.66, 36.32, and 28.55. MALDI-MS $[\text{M}+\text{H}]^+$ ($\text{C}_{174}\text{H}_{319}\text{N}_{16}\text{O}_{114}$) calc m/z = 4456.96543. Found m/z = 4463.499.

(Melibiose) $_6$ -GD (Compound 18d): Compound 4 (13.8 mg, 0.0164 mmol), 11 (63.7 mg, 0.111 mmol), TBTU (75.8 mg, 0.236 mmol), DIPEA ($\text{pH}\approx 9$ –10), and DMSO (1 mL) were utilized. 32.7 mg (0.0094 mmol, 57%) of an off-white fluffy solid resulted after purification. ^1H NMR (500 MHz, D_2O): δ 7.59 (d, 1H, J = 6.5 Hz, E isomer), 6.94 (d, 0.2H, J = 6.3 Hz, Z isomer), 4.98 (app d, 2H, J = 3.6 Hz), 4.42 (t, 1H, J = 6.7 Hz), 4.29 (m, 0.3H), 4.24 (br m, 3.2H), 3.99 (m, 5H), 3.95–3.87 (m, 5.5H), 3.83 (m, 2.4H), 3.75 (m, 12.4H), 3.68 (m, 3.6H), 3.59 (m, 9.3H), 3.26 (t, 4H, J = 6.6 Hz), 2.77 (br app s, 4.5H), 2.66 (br app d, 4.5H), 2.51 (t, 4H, J = 5.5 Hz), and 1.80 (app t, 4H, J = 6.5 Hz). ^{13}C NMR (125 MHz, D_2O with internal MeOH std.): δ 174.00, 161.81, 152.85, 151.76, 98.58, 77.17, 75.97, 73.63, 73.26, 72.93, 71.17, 71.05, 70.58, 70.51, 70.39, 70.01, 69.78, 69.67, 69.54, 69.48, 68.94, 68.79, 68.73, 68.68, 68.52, 68.28, 67.02, 66.82, 66.62, 61.37, 61.32, 53.19, 51.46, 51.09, 36.66, 36.41, and 28.55. MALDI-MS $[\text{M}+\text{H}]^+$ ($\text{C}_{138}\text{H}_{259}\text{N}_{16}\text{O}_{84}$) calc m/z = 3484.64815. Found m/z = 3484.64550.

General Procedure for the Formation of Sulfo-(Sugar) $_6$ -SGDs (12e–18e): The sulfation reactions were carried out as reported previously.^[11a] Briefly, 1 equiv. of each GD (12d–18d) was weighed into an oven-dried flask and dissolved in 2.5–3.0 mL of DriSolv DMF (*N,N*-dimethylformamide). Next, the flask was placed under N_2 (g) and a large excess (126 equiv.) of sulfur trioxide pyridine complex was added dropwise to the reaction mixture. The reactions were terminated by adding 1.0 mL of ice-cold water and adjusting the pH to above 9.0 with 2M NaOH. The solution was then added dropwise to ice-cold acetone and left to precipitate at -20°C for 24 h. The precipitate was collected by centrifugation, re-dissolved in a minimum amount of water, and then dialyzed against water in 2000 MWCO tubing. FPLC was utilized as a final purification step. The resultant peaks were pooled separately and freeze-dried. The SGDs (12e–18e) were characterized by NMR and the % sulfur determined by elemental analysis. Using the carbon and nitrogen content from the MS data for the GDs, the %S, the molecular formula, the total number of sulfate groups and the number of sulfates/sugar residue were determined for the SGDs.

(Cellobiose) $_6$ -SGD (Compound 12e): Compound 12d (17.6 mg, 0.0051 mmol) and SO_3 -pyr (101.1 mg, 0.637 mmol), and DMF (2.5 mL) were combined as described. After purification, 17.4 mg (0.0034 mmol, 67%) of a yellowish amorphous solid was obtained. Elemental analysis revealed 12.56% sulfur, with an approximate molecular formula of $\text{C}_{138}\text{H}_{238}\text{N}_{16}\text{S}_{20}\text{O}_{144}$, and molecular weight of 5061 g mol^{-1} . ^1H NMR (500 MHz, D_2O): δ 4.54 (m, 5H), 4.25 (m, 12H), 3.99 (br app t, 1H), 3.81 (m, 17H), 3.61 (br s, 5H), 3.44 (br s, 5H), 3.35 (br s, 3H), 3.24 (br app t, 5H), 2.97 (m, 3H), 2.56 (br s, 4H), and 1.80 (br s, 4H).

(GlcNAc) $_6$ -SGD (Compound 13e): Compound 13d (29.8 mg, 0.0108 mmol) and SO_3 -pyr (123.8 mg, 0.778 mmol), and DMF (2.5 mL) were combined as described. After purification, 18.0 mg (0.0052 mmol, 48%) of a yellowish amorphous solid was obtained. Elemental analysis revealed 8.66% sulfur, with an approximate molecular formula of $\text{C}_{114}\text{H}_{207}\text{N}_{22}\text{S}_9\text{O}_{81}$, and molecular weight of 3484 g mol^{-1} . ^1H NMR (500 MHz, D_2O): δ 7.63 (br app d, 0.3H), 7.54 (br s, 0.3H), 5.18 (br s, 0.1H), 5.10 (br m, 0.3H), 4.97 (br s, 0.1H), 4.90 (br s, 0.1H), 4.65 (br app d, 0.3H), 4.58 (m, 0.4H), 4.46 (m, 1H), 4.35–4.17 (m, 5H), 4.07 (br app d, 1H), 3.85–3.74 (m, 14H), 3.62 (br app s, 5H), 3.45 (br app d, 7H), 3.27 (br app d, 5H), 3.03 (br s, 3H), 2.95 (d, 1H, J = 5.3 Hz), 2.54 (br app s, 5H), 2.02 (s, 3H, NHAc), and 1.79 (br app t, 4H, J = 5.9 Hz).

(Gentiobiose) $_6$ -SGD (Compound 14e): Compound 14d (10.4 mg, 0.0030 mmol) and SO_3 -pyr (60.3 mg, 0.379 mmol), and DMF (2.5 mL) were combined as described. After purification, 10.5 mg (0.0025 mmol, 82%) of a fluffy white solid was obtained. Elemental analysis revealed 7.0%

sulfur, with an approximate molecular formula of $C_{138}H_{248}N_{16}S_{10}O_{114}$, and molecular weight of 4260 g mol^{-1} . $^1\text{H NMR}$ (500 MHz, D_2O): δ 4.61 (m, 2.5H), 4.46 (m, 2.3H), 4.22 (m, 9H), 3.92 (m, 4H), 3.74 (br app d, 15H), 3.60 (br s, 6H), 3.26 (br app d, 6H), 2.93 (br s, 3H), 2.54 (br s, 5H), and 1.80 (br s, 4H).

(Lactose)₆-SGD (Compound 15e): Compound 15d (18.1 mg, 0.0052 mmol) and SO_3 -pyr (104.2 mg, 0.655 mmol), and DMF (2.5 mL) were combined as described. After purification, 17.4 mg (0.0033 mmol, 64%) of a yellowish amorphous solid was obtained. Elemental analysis revealed 13.41% sulfur, with an approximate molecular formula of $C_{138}H_{236}N_{16}S_{22}O_{150}$, and molecular weight of 5219 g mol^{-1} . $^1\text{H NMR}$ (500 MHz, D_2O): δ 7.81 (m, 0.4H), 7.72 (m, 0.6H), 5.29 (m, 0.3H), 5.20 (br m, 0.6H), 5.11 (br app d, 0.4H), 5.02 (br m, 0.7H), 4.57 (m, 2H), 4.46–4.15 (m, 15H), 3.99 (m, 2H), 3.87–3.73 (m, 15H), 3.63 (br app d, 5H, $J = 5.4 \text{ Hz}$), 3.52 (br s, 4H), 3.41 (br s, 2H), 3.29 (br s, 4H) 3.01 (m, 3H), 2.57 (br s, 4H), and 1.81 (br app t, 4H, $J = 6.3 \text{ Hz}$).

(Maltose)₆-SGD (Compound 16e): Compound 16d (14.9 mg, 0.0043 mmol) and SO_3 -pyr (86.6 mg, 0.542 mmol), and DMF (2.5 mL) were combined as described. After purification, 13.4 mg (0.0027 mmol, 65%) of a fluffy white solid was obtained. Elemental analysis revealed 11.8% sulfur, with an approximate molecular formula of $C_{138}H_{240}N_{16}S_{18}O_{138}$, and molecular weight of 4911 g mol^{-1} . $^1\text{H NMR}$ (500 MHz, D_2O): δ 4.61 (m, 1H), 4.44–4.17 (m, 18H), 3.87–3.74 (m, 16H), 3.61 (br m, 5H), 3.53 (br s, 4H), 3.44 (br s, 2H), 3.29 (br app d, 4H, $J = 6.8 \text{ Hz}$), 3.06 (br s, 2H), 2.56 (br s, 4H), and 1.81 (br s, 4H).

(Maltotriose)₆-SGD (Compound 17e): Compound 17d (20.5 mg, 0.0046 mmol) and SO_3 -pyr (133.7 mg, 0.840 mmol), and DMF (2.5 mL) were combined as described. After purification, 22.3 mg (0.0034 mmol, 74%) of a fluffy white solid was obtained. Elemental analysis revealed 13.0% sulfur, with an approximate molecular formula of $C_{174}H_{291}N_{16}S_{27}O_{195}$, and molecular weight of 6583 g mol^{-1} . $^1\text{H NMR}$ (500 MHz, D_2O): δ 4.58 (m, 1.5H), 4.41–4.16 (m, 20H), 4.05 (m, 3H), 3.81 (m, 18H), 3.57 (m, 10H), 3.44 (br app s, 3H), 3.27 (br app d, 4H, $J = 7.7 \text{ Hz}$), 3.06 (br s, 2H), 2.57 (br s, 4H), and 1.80 (br s, 4H).

(Melibiose)₆-SGD (Compound 18e): Compound 18d (19.2 mg, 0.0055 mmol) and SO_3 -pyr (110.6 mg, 0.695 mmol), and DMF (2.5 mL) were combined as described. After purification, 22.2 mg (0.0046 mmol, 84%) of a yellowish amorphous solid was obtained. Elemental analysis revealed 11.23% sulfur, with an approximate molecular formula of $C_{138}H_{241}N_{16}S_{17}O_{135}$, and molecular weight of 4826 g mol^{-1} . $^1\text{H NMR}$ (500 MHz, D_2O): δ 7.73–7.56 (m, 1H), 5.35 (br m, 1.4H), 5.10 (s, 0.6H), 5.00 (d, 0.2H, $J = 3.8 \text{ Hz}$), 4.93 (t, 0.4H, $J = 7.7 \text{ Hz}$), 4.67 (m, 1H), 4.58 (m, 2H), 4.45 (m, 2.3H), 4.29–4.19 (m, 8H), 4.03 (m, 3H), 3.87–3.73 (m, 16H), 3.59 (m, 10H), 3.42 (br s, 3H), 3.27 (br app d, 4H, $J = 6.9 \text{ Hz}$), 3.07 (br m, 2H), 2.56 (br s, 4H), and 1.80 (br s, 4H).

ELISA Assay: A competitive format ELISA was developed using Ni²⁺ coated 96 well strip plates and HIV-1 AC10.29 gp120 Avi-His Recombinant Protein (Cat. #13 055, NIH AIDS Reagent Program). This protein contains a (His)₆ tag at the C-terminal end. Initially, the assay plate was washed 3 × 300 μL with PBS x 0.05% (v/v) Tween-20 (PBST). Next, the gp120 was diluted 1:1000 in PBS buffer and 100 μL was added to each well. The plate was covered and incubated at 4 °C in the dark overnight. Next, the plate was incubated for 1 additional hour at 25 °C in a jitterbug shaker incubator (mix setting of 5) to ensure maximum capture of the gp120 protein. After the incubation, the plate was washed 3 × 250 μL with PBST. Serial dilutions of each SGD or the positive control (DS) were prepared in PBS (0.2–800 $\mu\text{g mL}^{-1}$). 50 μL /well of each dilution was added in duplicate wells. There were also 2 wells/analyte of 0 $\mu\text{g mL}^{-1}$ and 2 wells/analyte of a negative control (no added antibody), these wells received 50 μL /well of PBS in place of an SGD dilution. Next, 50 μL /well of a 1:1000 dilution of HRP-labeled anti-V3 loop monoclonal antibody (mAb, Cat. #1101-P, Immunodx) was added to all wells except the negative control, which received 50 μL /well of PBS. This resulted in a 1:2 dilution of both the SGDs (0.1–400 $\mu\text{g mL}^{-1}$) and the HRP-mAb (1:2000 final dilution). The plate was covered and incubated for 1 h at 25 °C, with a shake setting of 5, followed by another wash step as before. The plate was developed by added 100 μL /well of Sureblue TMB and reading the plate 1x/minute at 655 nm in a BioRad model 680 microplate reader for 15 min (step read, mix low), upon which,

100 μL /well of 1M HCl was added to stop the color development. The plate was read once more at 450 nm (fast read) to provide the endpoint absorbance values. These readings were normalized through subtraction of the average absorbance of the negative control wells, then transferred to GraphPad Prism 9.0 where a non-linear dose-response curve was generated and an IC₅₀ value calculated. Each IC₅₀ value was generated from a minimum of two replicates of the assay.

MST Assay: All MST experiments were conducted on a Monolith NT.115 instrument from NanoTemper using 40% excitation power and the medium IR intensity setting. Samples were dissolved or diluted in 10 mM sodium phosphate buffer, pH 7. (His)₆-gp120 (HIV-1 AC10.29 gp120 Avi-His Recombinant Protein, Cat. #13 055, NIH AIDS Reagent Program) was modified with the Monolith NT His-Tag Labeling Kit RED-tris-NTA from NanoTemper (cat. no. L008). Because the Avi-His tag was at the C-terminus region of gp120, attachment of the fluorescent NT-647 dye should not interfere with the direct binding of SGDs. The labeled gp120 (200 nm) was incubated with 50 000 to 0.01 nmol SGD, as obtained by serial dilution. DS (500 000 g mol^{-1}) was used as a positive binding control. Once incubated for an additional five minutes after mixing, each solution was loaded in standard MST quartz capillary tubes and placed in the instrument to examine the thermophoresis response at 25 °C. Binding results were plotted and quantified with the MO. Affinity Analysis software (v2.2.7) was provided by NanoTemper. This software allowed the user to fit the data to a dissociation constant (K_d), assuming the thermophoresis response of the bound and unbound species were significantly different. The optimum “hot region” was selected as the 4–5 s window by the software.

HIV-1 Neutralization Luciferase Reporter Gene Assay: The HIV-1 neutralization assays were performed using TZM-bl cells, according to the method Montefiori et al. at Duke University in the Good Clinical Laboratory Practice (GCLP)-compliant Laboratory for AIDS Vaccine Research and Development.^[11b] Briefly, HIV inhibition was measured in 96-well culture plates by using Tat-regulated luciferase (Luc) reporter gene expression to quantify reductions in virus infection in TZM-bl cells. Assays were performed with HIV-1 Env-pseudotyped viruses Q23.17 (Clade A), MN.3 (Clade B), MW965.26 (Clade C), and TV1.21 (Clade C). The positive controls used in the neutralization assays were 500 kDa DS and the IgG antibody CH01-31, as reported previously.^[11] Samples of the SGDs and DS were prepared as follows: SGDs were dissolved in PBS, sterile-filtered to give 1 mg mL⁻¹ concentrated stock solutions, then serially diluted to give concentrations ranging either from 0.02 to 50 $\mu\text{g mL}^{-1}$ or 0.02–25 $\mu\text{g mL}^{-1}$. Diluted SGDs were pre-incubated with the virus (≈ 150 000 relative light unit equivalents) for 1 h at 37 °C before the addition of TZM-bl cells. Following an additional 48 h incubation, cells were lysed and Luc activity was determined using a microtiter plate luminometer and BriteLite Plus Reagent (Perkin Elmer). Neutralization titers were the SGD concentration at which relative luminescence units (RLU) were reduced by 50% compared to RLU in virus control wells after subtraction of background RLU in cell control wells.

Cytotoxicity Assay: The cytotoxicity profiles of the SGDs were performed using the CellTiter-Glo Luminescent Cell Viability Assay, by Promega.^[24] The cell viability assay was performed in a 96-well plate. SGDs were prepared in 150 $\mu\text{g mL}^{-1}$ stock solutions, then serially diluted to concentrations ranging from 0.02–50 $\mu\text{g mL}^{-1}$ or 0.02–25 $\mu\text{g mL}^{-1}$. Solid CellTiter-Glo Substrate was reconstituted in CellTiter-Glo Buffer to form the CellTiter-Glo Reagent at room temperature. The TZM-bl cell cultures (100 μL per well) were incubated at 37 °C for 24 h in the presence of various concentrations of SGDs (from 0.02–50 $\mu\text{g mL}^{-1}$). CellTiter-Glo Reagent was then added at 100 μL to each well. The plate was mixed using an orbital shaker for 2 min to induce cell lysis, then incubated at room temperature for 10 min to stabilize the luminescent signal. The luminescent signal was measured using a microtiter plate luminometer, and the percent of viable cells was determined using the protocol provided by the manufacturer.

MD Simulations (HIV Trimeric gp120): In order to check the experimentally observed binding between SGDs and gp120, these systems were modeled by atomistic molecular dynamics simulations using NAMD.^[25] In the simulations, the gp120 protein complex used was a trimer based on PDB code 5V8M.^[26] Its V3 loop, a principle neutralizing domain

with amino acids 303–338, is known to bind with a host cell surface via HSPGs.^[11a] Four oxime-linked hexavalent SGDs displaying high inhibitory activities in *in vitro* inhibition of infectivity assays were selected to simulate the interaction with gp120. Having the same dendritic core, the four glyco-dendrimers differed by their terminal groups, which included: cellobiose, lactose, maltotriose, and melibiose. The sulfated (SGDs: 12e, 15e, 17e, and 18e) and non-sulfated states (GD: 12d, 15e, 17e, and 18e) of the four molecules were also considered, which gave eight simulated systems. The sulfate groups were mostly added to C6 of each sugar unit, according to the average number of sulfates per sugar. Here, the average number of sulfates was 1.6/sugar (cellobiose, 12e), 1.8/sugar (lactose, 15e), 1/sugar (maltotriose, 17e), and 1.3/sugar (melibiose, 18e). The DS was used as a positive control, while the four GDs work as negative controls. All the systems were immersed in 150 mM NaCl solutions.

MD Simulations (SARS-CoV-2 Monomeric RBD): Since the new coronavirus, SARS-CoV-2, also has an HSPG binding site, Lactose SGD and GDs (15d and 15e) and Cellobiose SGD and GD (12d and 12e) were selected to test their binding with the RBD (PDB:12216M17) of SARS-CoV-2. The four GDs were separately placed around the top and middle part of RBD with two trials for each case. The top region was the binding site of ACE2, which was the cellular receptor of SARS-CoV-2,^[22] and the middle part contained the exposed basic regions which could be the binding site for HSPG. In addition, two types of hybrid compounds with an octavalent core functionalized by half SGD and half GD were also designed to examine the binding strength.

Simulation Methods: All the systems were immersed in 150 mM NaCl solutions. Different GDs were named by their sugar functional groups. The simulations were performed for 100–200 ns for gp120 systems and 70–100 ns for SARS-CoV-2 systems, with a slight difference due to the computer power and time needed to reach equilibrium. The gp120 and RBD of SARS-CoV-2 proteins were described by a CHARMM36^[27] force field, while GDs were described by a CHARMM general force field.^[28] The Particle Mesh Ewald (PME)^[29] method was used for the evaluation of long-range Coulombic interactions. The time step was set to 2.0 fs. The simulations were performed by NAMD^[25] in the NPT ensemble ($p = 1$ bar and $T = 300$ K), using the Langevin dynamics ($\gamma_{\text{Lang}} = 1$ ps⁻¹). After 2000 steps of minimization, ions and water molecules were equilibrated for 2 ns around protein and GDs, which were restrained using harmonic forces with a spring constant of 1 kcal (mol Å²)⁻¹. The last frames of restrained equilibration were used to start simulations of free GDs and partially constrained protein (the part on the bottom). The trajectories and snapshots were visualized by VMD.^[30] The MM-GBSA free energy^[31] of binding between compounds and protein targets were evaluated by NAMD^[25] in a generalized Born Implicit Solvent (150 mM). The averaged MM-GBSA free energy was taken from the last 20 ns (500 frames) of each simulation.

Statistics: For each of the *in vitro* assays, the statistical treatment of the data is as described below.

ELISA: ELISA data were collected in duplicate for each concentration of the SGD tested, and each assay was replicated a minimum of twice per compound. For the analysis, the endpoint absorbances at 450 nm were first corrected by subtracting the average of the duplicate blank wells, and second, the duplicate data points were averaged. The averaged data points for each concentration of SGD (0–0.4 g L⁻¹) were then imported into GraphPad Prism 9.0 software and subjected to a sigmoidal dose-response least squares fit. The 0 g L⁻¹ data point was set to a concentration of 1×10^{-8} g L⁻¹ so it could be included in the analysis. The program plots the data as the Absorbance at 450 nm versus the log of the SGD concentration (g L⁻¹). The R² value for each assay was used to determine the goodness of fit for a given SGD. SGDs that provided R² values >0.9 were retained and reported. Any SGD giving reproducible R² values <0.9 were reported as having an IC₅₀ value of >[highest conc.]. This assay was utilized as a semi-quantitative screening assay, to determine whether further biological testing should be undertaken (go/no go), so no statistical analysis was conducted.

MST: MST data were collected in triplicate for each ligand tested and analyzed with the software provided by the instrument manufacturer (NanoTemper Technologies, MO. Affinity Analysis v2.2.7). For all samples, the initial fluorescence prior to heating was normalized to 1.0 unit = 1000 %

(per mille). The drop in fluorescence at a set time point after heating was plotted on the y-axis of the binding curve and denoted FNorm [%]. Error bars for the data points in the MST binding curves were calculated as the standard deviation, but were omitted in Figure 3 for clarity. See Figure S39, panel C, Supporting Information, for typical result with error bars included. The error in each K_d value, as reported in the third column of Figure 2, was obtained from the confidence in the binding fit to an ideal interaction of 1:1 binding stoichiometry and was calculated by the NanoTemper analysis software.

HIV-1 Neutralization Luciferase Reporter Gene Assay: The HIV-1 neutralization luciferase reporter gene assay has been formally optimized and validated.^[32] Each analyte concentration was tested in duplicate. As this was a biological assay with inherent variability, the analyzed compounds were judged as having antiviral activity if the “with antibody/compound” results were more than threefold different from the “without antibody/compound” result. The assays on early-stage compounds were conducted only once due to resource constraints, so no statistical analysis was carried out.

Cytotoxicity Assay: This assay was conducted according to the instructions provided by Promega.

Supporting Information

Supporting Information is available from the Wiley Online Library or from the author.

Acknowledgements

The authors acknowledge the following support for this work: NIH-SCORE 5SC3GM119521 (K.D.M.), NIAID-NIH Contract Number: HHSN272201800004C (C.C.L.), NSF-MRI (500 MHz NMR spectrometer, MPS-0922676 (KDM) and MST instrument DBI-1427465 (D.K.E.)), CSUPERB (California State University Program for Education and Research in Biotechnology) Research Development Award (K.D.M.), UIC Center for Clinical and Translational Science (P.K. and Y.H.), UIC Dean's Scholar Fellowship (Y.H.), and the CSUS Department of Chemistry Russell-Forkey summer research fellowship (L.W.). Mass spectrometry was conducted at The Ohio State University Campus Chemical Instrument Center (CCIC) and acknowledges the following support for this facility: NIH Award Number P30 CA016058, NIH Award Number 1 S10 RR025660-01A1, and NIH Award Number Grant S10 OD018507. The HIV-1 AC10.29 gp120 Avi-His Recombinant Protein (Cat #: 13055) was obtained through the NIH AIDS Reagent Program, Division of AIDS, NIAID, from Dr. Xueling Wu. T2M-bl cells were obtained from the NIH AIDS Reagent Program, as contributed by John Kappes and Xiaoyun Wu. Finally, the authors thank R. Anthony Perez for creating the MST image in Figure 3.

Conflict of Interest

The authors declare no conflict of interest.

Data Availability Statement

Research data are not shared.

Keywords

glycodendrimers, HIV-1, molecular dynamics, SARS-CoV-2 receptor binding domain

Received: September 16, 2020

Revised: January 4, 2021

Published online: February 12, 2021

- [1] UNAIDS, Fact Sheet-World AIDS Day, <https://www.unaids.org/en/resources/fact-sheet> (accessed: December 2020).
- [2] Worldometer, Coronavirus, <https://www.worldometers.info/coronavirus/> (accessed: December 2020).
- [3] CDC, Flu Vaccination Coverage, United States, 2018–19 Influenza Season, <https://www.cdc.gov/flu/fluview/coverage-1819estimates.htm> (accessed: May 2020).
- [4] K. M. Gibas, P. van den Berg, V. E. Powell, D. S. Krakower, *Drugs* **2019**, 79, 609.
- [5] a) D. Spillmann, *Biochimie* **2001**, 83, 811; b) Y. Choi, H. Chung, H. Jung, J. R. Couchman, E.-S. Oh, *Matrix Biol.* **2011**, 30, 93; c) E. Kamhi, E. J. Joo, J. S. Dordick, R. J. Linhardt, *Biological Rev.* **2013**, 88, 928; d) Y. Chen, M. Gotte, J. Liu, P. W. Park, *Mol. Cells* **2008**, 26, 415; e) J. Lang, N. Yang, J. Deng, K. Liu, P. Yang, G. Zhang, C. Jiang, *PLoS One* **2011**, 6, e23710; f) H. Hondermarck, N. W. Bartlett, V. Nurcombe, *FASEB BioAdv.* **2020**, 2, 296.
- [6] a) K. S. Rostand, J. D. Esko, *Infect. Immun.* **1997**, 65, 1; b) M. Moulard, H. Lortat-Jacob, I. Mondor, G. Roca, R. Wyatt, J. Sodroski, L. Zhao, W. Olson, P. D. Kwong, Q. J. Sattentau, *J. Virol.* **2000**, 74, 1948; c) D. Batinic, F. A. Robey, *J. Biol. Chem.* **1992**, 267, 6664.
- [7] a) W. Hao, B. Ma, Z. Li, X. Wang, X. Gao, Y. Li, B. Qin, S. Shang, S. Cui, Z. Tan, *bioRxiv* **2020**; b) S. Y. Kim, W. Jin, A. Sood, D. W. Montgomery, O. C. Grant, M. M. Fuster, L. Fu, J. S. Dordick, R. J. Woods, F. Zhang, R. J. Linhardt, *Antiviral Res.* **2020**, 181, 104873; c) C. Mycroft-West, D. Su, S. Elli, S. Guimond, G. Miller, J. Turnbull, E. Yates, M. Guerrini, D. Fernig, M. Lima, M. Skidmore, *bioRxiv* **2020**.
- [8] a) Y.-C. Lee, R. T. Lee, *Acc. Chem. Res.* **1995**, 28, 321; b) J. J. Lundquist, E. J. Toone, *Chem. Rev. (Washington, DC, U. S.)* **2002**, 102, 555; c) J. L. J. Blanco, C. O. Mellet, J. M. G. Fernández, *Chem. Soc. Rev.* **2013**, 42, 4518.
- [9] a) D. Sepulveda-Crespo, R. Cena-Diez, J. L. Jimenez, M. A. Muñoz-Fernández, *Med. Res. Rev.* **2017**, 37, 149; b) R. Cena-Diez, D. Sepulveda-Crespo, M. Maly, M. A. Munoz-Fernandez, *RSC Adv.* **2016**, 6, 46755.
- [10] Starpharma, VivaGel, https://www.starpharma.com/vivagel/vivagel_availability (accessed: January 2021).
- [11] a) R. Clayton, J. Hardman, C. C. LaBranche, K. D. McReynolds, *Bioconjugate Chem.* **2011**, 22, 2186; b) D. C. Montefiori, in *HIV Protocols, Second Edition, Vol. 485*, (Eds.: V. R. Prasad, G. V. Kalpana, Humana Press, New York **2009**, pp. 395–404.
- [12] K. D. McReynolds, D. Dimas, H. A. Le, *Tetrahedron Lett.* **2014**, 55, 2270.
- [13] M. Nakamura, T. Sanji, M. Tanaka, *Chem. Eur. J.* **2011**, 17, 5344.
- [14] K. McReynolds, D. Dimas, G. Floyd, K. Zeman, *Pharmaceuticals* **2019**, 12, 39.
- [15] a) S. A. I. Seidel, P. M. Dijkman, W. A. Lea, G. van den Bogaart, M. Jerabek-Willemsen, A. Lazic, J. S. Joseph, P. Srinivasan, P. Baaske, A. Simeonov, I. Katritch, F. A. Melo, J. E. Labdury, G. Schreiber, A. Watts, D. Braun, S. Dühr, *Methods* **2013**, 59, 301; b) M. Asmari, R. Ratih, H. A. Alhazmi, S. E. Deeb, *Methods* **2018**, 146, 107.
- [16] D. Sepulveda-Crespo, R. Gomez, F. J. De La Mata, J. L. Jimenez, M. A. Muñoz-Fernández, *Nanomedicine* **2015**, 11, 1481.
- [17] D. Tyssen, S. A. Henderson, A. Johnson, J. Sterjovski, K. Moore, J. La, M. Zanin, S. Secondo, P. Karellas, M. P. Giannis, G. Krippner, S. Wessellingh, T. McCarthy, P. R. Gorry, P. A. Ramsland, R. Cone, J. R. A. Paull, G. R. Lewis, G. Tachedjian, *PLoS One* **2010**, 5, e12309.
- [18] R. D. Kensinger, B. J. Catalone, F. C. Krebs, B. Wigdahl, C.-L. Schengrund, *Antimicrob. Agents Chemother.* **2004**, 48, 1614.
- [19] a) M. Ito, M. Baba, A. Sato, R. Pauwels, E. De Clercq, S. Shigeta, *Antiviral Res.* **1987**, 7, 361; b) M. Baba, R. Pauwels, J. Balzarini, J. Arnout, J. Desmyter, E. De Clercq, *Proc. Natl. Acad. Sci. USA* **1988**, 85, 6132; c) K. J. Lorentson, C. W. Hendrix, J. M. Collins, D. M. Kornhauser, B. G. Petty, R. W. Klecker, C. Flexner, R. H. Eckel, P. S. Lietman, *Ann. Intern. Med.* **1989**, 111, 561.
- [20] a) J. M. Stauber, E. A. Qian, Y. Han, A. L. Rheingold, P. Kral, D. Fujita, A. M. Spokoyny, *J. Am. Chem. Soc.* **2020**, 142, 327; b) E. A. Qian, Y. Han, M. S. Messina, H. D. Maynard, P. Kral, A. M. Spokoyny, *Bioconjugate Chem.* **2019**, 30, 2594; c) E. A. Qian, A. I. Wixtrom, J. C. Axtell, A. Saebi, D. Jung, P. Rehak, Y. Han, E. H. Moully, D. Mosallaei, S. Chow, M. S. Messina, J. Y. Wang, A. T. Royappa, A. L. Rheingold, H. D. Maynard, P. Král, A. M. Spokoyny, *Nat. Chem.* **2017**, 9, 333; d) V. Cagno, P. Andreozzi, M. D'Alicarnasso, P. Jacob Silva, M. Mueller, M. Galloux, R. Le Goffic, S. T. Jones, M. Vallino, J. Hodek, J. Weber, S. Sen, E. R. Janecek, A. Bekdemir, B. Sanavio, C. Martinelli, M. Donalizio, M. A. Rameix Welti, J. F. Eleouet, Y. Han, L. Kaiser, L. Vukovic, C. Tapparel, P. Kral, S. Krol, D. Lembo, F. Stellacci, *Nat. Mater.* **2018**, 17, 195; e) S. Sen, Y. Han, P. Rehak, L. Vuković, P. Král, *Chem. Soc. Rev.* **2018**, 47, 3849.
- [21] H. Feinberg, R. Castelli, K. Drickamer, P. H. Seeberger, W. I. Weis, *J. Biol. Chem.* **2007**, 282, 4202.
- [22] R. Yan, Y. Zhang, Y. Li, L. Xia, Y. Guo, Q. Zhou, *Science* **2020**, 367, 1444.
- [23] S. T. Jones, V. Cagno, M. Janeček, D. Ortiz, N. Gasilova, J. Piret, M. Gasbarri, D. A. Constant, Y. Han, L. Vuković, P. Král, L. Kaiser, S. Huang, S. Constant, K. Kirkegaard, G. Boivin, F. Stellacci, C. Tapparel, *Sci. Adv.* **2020**, 6, eaax9318.
- [24] S. Cecioni, S. Faure, U. Darbost, I. Bonnamour, H. Parrot-Lopez, O. Roy, C. Taillefumier, M. Wimmerova, J.-P. Praly, A. Imbert, S. Vidal, *Chem. Eur. J.* **2011**, 17, 2146.
- [25] J. C. Phillips, R. Braun, W. Wang, J. Gumbart, E. Tajkhorshid, E. Villa, C. Chipot, R. D. Skell, L. Kale, K. Schulten, *J. Comp. Chem.* **2005**, 26, 1781.
- [26] J. H. Lee, R. Andrabi, C. Y. Su, A. Yasmeen, J. P. Julien, L. Kong, N. C. Wu, R. McBride, D. Sok, M. Pauthner, C. A. Cottrell, T. Nieuwsma, C. Blattner, J. C. Paulson, P. J. Klasse, I. A. Wilson, D. R. Burton, A. B. Ward, *Immunity* **2017**, 46, 690.
- [27] A. D. MacKerell Jr, D. Bashford, M. Bellott, R. L. Dunbrack Jr, J. D. Evanseck, M. J. Field, S. Fischer, J. Gao, H. Guo, S. Ha, D. Joseph-McCarthy, L. Kuchnir, K. Kuczera, F. T. K. Lau, C. Mattos, S. Michnick, T. Ngo, D. T. Nguyen, B. Prodhom, I. Reiher, *J. Phys. Chem. B* **1998**, 102, 3586.
- [28] K. Vanommeslaeghe, A. D. MacKerell Jr, *J. Chem. Inf. Model.* **2012**, 52, 3144.
- [29] T. Darden, D. York, L. Pedersen, *J. Chem. Phys.* **1993**, 98, 10089.
- [30] W. Humphrey, A. Dalke, K. Schulten, *J. Mol. Graphics* **1996**, 14, 33.
- [31] N. Homeyer, H. Gohlke, *Mol. Inform.* **2012**, 31, 114.
- [32] M. Sarzotti-Kelsoe, R. T. Bailer, E. Turk, C.-L. Lin, M. Bilska, K. M. Greene, H. Gao, C. A. Todd, D. A. Ozaki, M. S. Seaman, J. R. Mascola, D. C. Montefiori, *J. Immunol. Methods* **2014**, 409, 131.